Lorentz gas with thermostatted walls

N. Chernov and D. Dolgopyat

Abstract. In a planar periodic Lorentz gas, a point particle (electron) moves freely and collides with fixed round obstacles (ions). If a constant force (induced by an electric field) acts on the particle, the latter will accelerate, and its speed will approach infinity [13, 14]. To keep the kinetic energy bounded one can apply a Gaussian thermostat, which forces the particle's speed to be constant. Then an electric current sets in and one can prove Ohm's law and the Einstein relation [15, 18, 19]. However, the Gaussian thermostat has been criticized as unrealistic, because it acts all the time, even during the free flights between collisions. We propose a new model, where during the free flights the electron accelerates, but at the collisions with ions its total energy is reset to a fixed level; thus our thermostat is restricted to the surface of the scatterers (the 'walls'). We rederive all physically interesting facts proven for the Gaussian thermostat in [15, 18, 19], including Ohm's law and the Einstein relation. In addition, we investigate the superconductivity phenomenon in the infinite horizon case.

Mathematics Subject Classification (2010). Primary 37D50; Secondary 82C70.

Keywords. Lorentz gas, thermostat, electrical current, Ohm's law, Einstein relation, diffusion, superconductivity.

1. Introduction and historic overview

We study a two-dimensional periodic Lorentz gas. It consists of a particle that moves on a plane between a periodic array of fixed scatterers (the latter are disjoint convex domains with C^3 boundaries). The particle bounces off the scatterers according to the rule 'the angle of incidence is equal to the angle of reflection'. The particle may be subject to an external force; see Fig. 1. Lorentz gas models the motion of electrons in metals [25].

The authors are grateful to the anonymous referees for many useful remarks and suggestions. N. Chernov acknowledges the hospitality of the University of Maryland. N. Chernov was partially supported by NSF grant DMS-0652896. D. Dolgopyat was partially supported by NSF grant DMS-0555743.

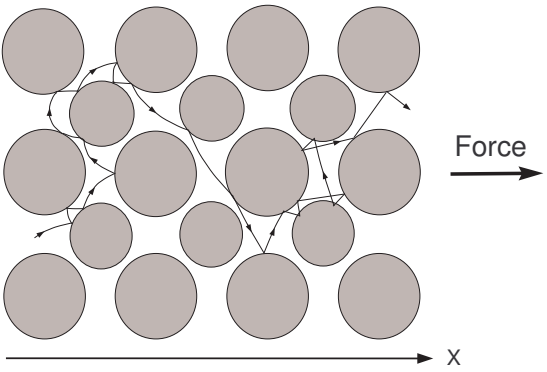

FIGURE 1. Lorentz gas with a finite horizon and an external force.

We denote by $\tilde{\mathcal{D}}$ the area available to the moving particle, i.e. the plane $\mathbb{R}^2$ minus the union of all the scatterers. Due to the periodicity, the plane can be covered by replicas of a fundamental domain (unit cell) $\mathcal{K} \subset \mathbb{R}^2$ so that $\tilde{\mathcal{D}}$ is the union of disjoint copies of $\mathcal{D} = \tilde{\mathcal{D}} \cap \mathcal{K}$. We denote those copies by $\mathcal{D}_i$ (we number them arbitrarily), i.e. $\tilde{\mathcal{D}} = \cup_i \mathcal{D}_i$. Let $\tilde{\pi}$ denote the natural projection of $\tilde{\mathcal{D}}$ onto $\mathcal{D}$. We will use tildas for objects on the unbounded table. In particular, we denote points in $\tilde{\mathcal{D}}$ by $\tilde{\mathbf{q}}$ and those in $\mathcal{D}$ by $\mathbf{q}$.

Lorentz gases without external forces. First we review some known facts. Suppose the particle moves freely between collisions, then its speed remains constant (and we set it to unity). Due to the periodicity of $\tilde{\mathcal{D}}$, the trajectory of the particle can be projected onto $\mathcal{D}$, and one gets a billiard in the compact table $\mathcal{D}$ with periodic boundary conditions. It is known as Sinai billiard and has been intensively studied since 1970; see [29].

Let $\mathbf{q} = \mathbf{q}(t)$ denote the position and $\mathbf{v} = d\mathbf{q}/dt$ the velocity of the moving particle in $\mathcal{D}$. Since $\|\mathbf{v}\| = 1$, the phase space is a 3D compact manifold $\Omega = \mathcal{D} \times \mathbb{S}^1$. The resulting flow Φ^t on Ω is Hamiltonian; it preserves the Liouville measure μ, which has a uniform density on Ω.

It is common to study flows by using a cross-section and the respective return map. In billiards, those can be constructed naturally on the collision space

$$\mathcal{M} = \big\{(\mathbf{q}, \mathbf{v})\colon \mathbf{q} \in \partial\mathcal{D},\ \|\mathbf{v}\| = 1,\ \mathbf{v} \text{ points inside } \mathcal{D}\big\}$$

consisting of all post-collisional vectors. The return map $\mathcal{F}\colon \mathcal{M} \to \mathcal{M}$ takes the particle right after a collision to its state right after the next collision; $\mathcal{F}$ is called the *collision map*.

We use the standard coordinates (r, φ) in $\mathcal{M}$, where r is the arc length parameter on $\partial\mathcal{D}$ and $\varphi \in [-\pi/2, \pi/2]$ the angle between the outgoing velocity vector $\mathbf{v}$ and the outward normal to $\partial\mathcal{D}$ at the collision point $\mathbf{q}$; cf. [7, 17] and Figure 3 below. The map $\mathcal{F}$ preserves a smooth probability measure ν

on $\mathcal{M}$ given by

$$d\nu = c_\nu \cos\varphi \, dr \, d\varphi, \qquad c_\nu = \big[2 \cdot \text{length}(\partial\mathcal{D})\big]^{-1} \tag{1.1}$$

here c_ν is just the normalizing factor. For every $X = (\mathbf{q}, \mathbf{v}) \in \mathcal{M}$ let

$$\tau(X) = \min\{t > 0 \colon \Phi^t(X) \in \mathcal{M}\} \tag{1.2}$$

denote the time of the first collision of the trajectory starting at X. Now Φ^t becomes a suspension flow constructed over the base map $\mathcal{F} \colon \mathcal{M} \to \mathcal{M}$ under the ceiling function τ.

Sinai proved [29] that the billiard flow Φ^t and the collision map $\mathcal{F}$ are hyperbolic (i.e. have non-zero Lyapunov exponents), ergodic, and K-mixing. Gallavotti and Ornstein [23] derived the Bernoulli property. Bunimovich and Sinai [6, 7] studied the Central Limit Theorem and other statistical laws. Young [31] and Chernov [8] established an exponential decay of correlations for the map $\mathcal{F}$; see [10] for bounds on correlations for the flow Φ^t. In other words, the Sinai billiards are highly chaotic in every mathematical sense.

Diffusion. We are mostly interested in the dynamics of the particle on the infinite table $\tilde{\mathcal{D}}$. We denote by $\tilde{\mathbf{q}}(t)$ the position of the moving particle in $\tilde{\mathcal{D}}$, and by $\tilde{\mathbf{q}}_n$ the point of its nth collision with $\partial\tilde{\mathcal{D}}$. Typically, both $\|\tilde{\mathbf{q}}(t)\|$ and $\|\tilde{\mathbf{q}}_n\|$ grow to infinity as time goes on.

Let $\mathbf{\Delta}_n = \tilde{\mathbf{q}}_{n+1} - \tilde{\mathbf{q}}_n$ denote the displacement vector between collisions. Note that $\tilde{\mathbf{q}}_n = \tilde{\mathbf{q}}_0 + \mathbf{\Delta}_0 + \mathbf{\Delta}_1 + \cdots + \mathbf{\Delta}_{n-1}$, thus based on the central limit theorem one may expect $\tilde{\mathbf{q}}_n/\sqrt{n}$ to converge to a normal distribution, which would be just a classical diffusion law. This indeed happens when the horizon is finite, i.e. when the free path between collisions with scatterers is bounded. Fig. 1 illustrates this situation – the scatterers are large enough to block the particle from all sides, so that it cannot move indefinitely without collisions. (We note however that Fig. 1 shows a trajectory affected by an external field, while in this subsection we describe a field-free model whose trajectories between collisions must be straight lines.)

Theorem 1 ([6, 7]**).** *Let $\tilde{\mathcal{D}}$ have finite horizon. Suppose that the initial position $\tilde{\mathbf{q}}(0)$ and velocity $\mathbf{v}(0)$ are chosen according to a smooth compactly supported probability measure. Then*
(a) *$\tilde{\mathbf{q}}_n/\sqrt{n}$ converges, as $n \to \infty$, to a normal distribution, i.e*

$$\tilde{\mathbf{q}}_n/\sqrt{n} \Rightarrow \mathcal{N}(\mathbf{0}, \mathbf{D})$$

with a non-degenerate covariance matrix $\mathbf{D}$ called diffusion matrix *given by the* Green-Kubo formula*:*

$$\mathbf{D} = \sum_{n=-\infty}^{\infty} \nu\big(\mathbf{\Delta}_0 \otimes \mathbf{\Delta}_n\big) \tag{1.3}$$

where $\mathbf{u} \otimes \mathbf{v}$ denotes the 'tensor product' of two vectors, i.e. the product of the column-vector $\mathbf{u}$ and the row-vector $\mathbf{v}$.
(b) *$\tilde{\mathbf{q}}(t)/\sqrt{t}$ converges, as $t \to \infty$, to another normal distribution,*

$$\tilde{\mathbf{q}}(t)/\sqrt{t} \Rightarrow \mathcal{N}(\mathbf{0}, \bar{\tau}^{-1}\mathbf{D})$$

where $\bar\tau = \nu(\tau)$ *is the mean free path given by*

$$\bar\tau = \nu(\tau) = \frac{\pi\,\mathrm{Area}(\mathcal{D})}{\mathrm{length}(\partial\mathcal{D})}. \tag{1.4}$$

The series (1.3) converges exponentially fast. See a recent exposition of these facts in [17, Chapter 7]; for the proof of (1.4) see [17, Section 2.13].

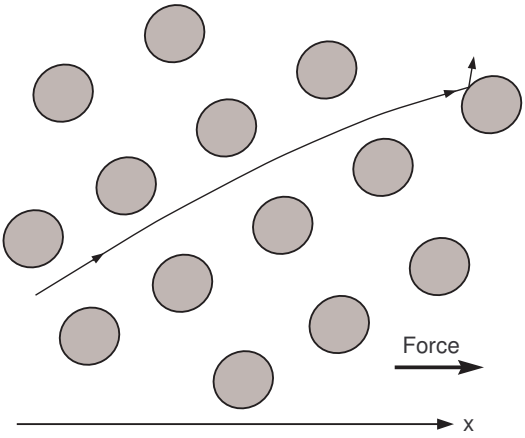

FIGURE 2. Lorentz gas with infinite horizon.

Super-diffusion. When the horizon is not finite, the particle can move freely without collisions along infinite corridors stretching between the scatterers, see Figure 2 (though see the remark before Theorem 1, it applies here, too). Now Theorem 1 cannot hold because the central term in the Green-Kubo series (1.3) diverges:

$$\nu\big(\mathbf{\Delta}_0 \otimes \mathbf{\Delta}_0\big) = \infty,$$

thus the diffusion matrix (1.3) turns infinite. In this case the particle exhibits an abnormal diffusion (often called 'superdiffusion'); namely the correct scaling factor is now $\sqrt{t\log t}$, rather than $\sqrt{t}$:

Theorem 2 ([30, 15]**).** *Let* $\tilde{\mathcal{D}}$ *have infinite horizon. Suppose that the initial position* $\tilde{\mathbf{q}}(0)$ *and velocity* $\mathbf{v}(0)$ *are chosen according to a smooth compactly supported probability measure. Then*
(a) *We have the following weak convergence, as* $n \to \infty$*:*

$$\frac{\tilde{\mathbf{q}}_n}{\sqrt{n\log n}} \Rightarrow \mathcal{N}(\mathbf{0}, \mathbf{D}_\infty),$$

where $\mathbf{D}_\infty$ *is called* superdiffusion matrix *given by the formula* (1.5) *below.* $\mathbf{D}_\infty$ *is non-degenerate iff there are two non-parallel corridors.*

(b) *We have the following weak convergence, as* $t \to \infty$*:*

$$\frac{\tilde{\mathbf{q}}(t)}{\sqrt{t \log t}} \Rightarrow \mathcal{N}(0, \bar{\tau}^{-1}\mathbf{D}_\infty),$$

where $\bar{\tau}$ *is again given by* (1.4).

The part (a) is proved by D. Szász and T. Varjú [30], the part (b) by the present authors [15]. The matrix $\mathbf{D}_\infty$ is given by a simple explicit formula in terms of the geometric characteristics of infinite corridors. Namely, suppose that each infinite corridor in $\tilde{\mathcal{D}}$ is bounded by two straight lines, each of which is tangent to an infinite row of scatterers that are copies of one scatterer in $\mathcal{D}$; then such lines are trajectories of some fixed points $X \in \mathcal{M}\colon \mathcal{F}(X) = X$ (one such point is shown in Figure 8). Now we have

$$\mathbf{D}_\infty = \sum_X \frac{c_\nu w_X^2}{2\,\|\boldsymbol{\Delta}(X)\|}\, \boldsymbol{\Delta}(X) \otimes \boldsymbol{\Delta}(X). \tag{1.5}$$

where the summation is taken over all corridors and all respective fixed points (note that there are four points X for each corridor). Here $\boldsymbol{\Delta}(X) = \boldsymbol{\Delta}_0(X)$ is the displacement vector of X introduced earlier and w_X is the width of the corridor bounded by the trajectory of X.

Lorentz gases under external forces. Suppose a constant force $\mathbf{E}$ acts on the particle, i.e. its motion is governed by equations

$$d\tilde{\mathbf{q}}/dt = \mathbf{v}, \qquad d\mathbf{v}/dt = \mathbf{E}. \tag{1.6}$$

It is common to interpret $\mathbf{E}$ as an electrical field that drives electrons and produces electrical current. Another popular physical model of this sort is Galton board [24]. It is commonly pictured as an upright wooden board with rows of pegs on which a ball rolls down under the gravitation force and bounces off the pegs. See recent studies in [13, 14].

For convenience we choose the coordinate system so that the x axis is aligned with the field, i.e. $\mathbf{E} = (E, 0)$ for some constant $E > 0$. Illustrations in Fig. 1 and Fig. 2 show the trajectories of the particle affected by an external force.

Equations (1.6) preserve the total energy

$$\tfrac{1}{2}\|\mathbf{v}\|^2 - \langle \mathbf{E}, \tilde{\mathbf{q}} \rangle = \mathcal{E} = \text{ const}. \tag{1.7}$$

In our coordinates the conservation law takes form

$$\tfrac{1}{2}\|\mathbf{v}\|^2 - Ex = \mathcal{E} = \text{ const}, \tag{1.8}$$

where x denotes the x-coordinate of the particle. As the particle is driven forward by the field, its x-coordinate grows, and so does its speed $v = \|\mathbf{v}\|$.

Despite the periodicity of the scatterers, the dynamics is not periodic, i.e. it is not a factor of any dynamical system in the domain $\mathcal{D}$ with periodic boundary conditions. In fact, the phase space $\tilde{\Omega}$ of the system is an unbounded 3D manifold

$$\tilde{\Omega}_\mathcal{E} = \{(\tilde{\mathbf{q}}, \mathbf{v})\colon \tilde{\mathbf{q}} = (x, y) \in \tilde{\mathcal{D}}, \quad \|\mathbf{v}\|^2 = 2(Ex + \mathcal{E})\}.$$

One can say that the motion of the particle on each domain $\mathcal{D}_i \subset \tilde{\mathcal{D}}$ depends on where $\mathcal{D}_i$ is located; more precisely it depends on the x-coordinate of points $\tilde{\mathbf{q}} \in \mathcal{D}_i$, the larger their x-coordinates, the faster the particle moves.

Suppose the particle is in $\mathcal{D}_i$ at time t_0, its x-coordinate is x_0 and its speed v_0 (it is roughly $v_0 \sim \sqrt{2Ex_0}$). If we change the time variable by $\hat{t} = v_0 t$, then the particle will have unit speed $\hat{v}_0 = 1$ at time $\hat{t}_0$ and it will move in a rescaled field $\hat{\mathbf{E}} = \mathbf{E}/v_0$. Otherwise its trajectory will be the same. Therefore we can approximate the particle's trajectories in the domain $\mathcal{D}_i$ with large x-coordinates by those of the particle moving in $\mathcal{D}$ with speed close to one, but in a weak external field.

In other words, the particle moves as if it always had unit speed but the field $\hat{\mathbf{E}}$ is space inhomogeneous – it gets weaker as the x-coordinate grows, so that $\hat{\mathbf{E}} = \mathcal{O}(1/\sqrt{x})$. Hence, as the particle moves on, it will behave more and more like a billiard particle. Since the net displacement of the latter is zero, the overall drift of our particle will tend to slow down.

As a result, the x-coordinate will *not* grow linearly in t. A detailed analysis shows that x will only grow as $t^{2/3}$, on average:

Theorem 3 ([13]**).** *Let $\tilde{\mathcal{D}}$ have finite horizon. Suppose that the initial position $\tilde{\mathbf{q}}(0)$ and velocity $\mathbf{v}(0)$ are chosen according to a smooth compactly supported measure on an energy surface $\{\mathcal{E} = \mathcal{E}_0\}$ where $\mathcal{E}_0$ is sufficiently large. Then there is a constant $c > 0$ such that $ct^{-2/3}x(t)$ converges, as $t \to \infty$, to a random variable with density*

$$\frac{3}{2\Gamma(2/3)} \exp\left[-z^{3/2}\right], \quad z \geq 0.$$

An explicit formula for c is given in [13, 15]. There exists a limiting distribution for $t^{-2/3}y(t)$, too, but it is given by a more complicated expression [14]. The extension of this theorem to tables $\tilde{\mathcal{D}}$ with infinite horizon remains an open problem. Our paper is motivated by an attempt to solve this problem – we believe our results will be useful.

Gaussian thermostat. Equations (1.6) and the resulting dynamics (Theorem 3) clearly do not give a realistic description of the electrical current – the real electrons do not accelerate indefinitely, and their average drift must be linear in t. To keep the energy of the moving particle fixed (and to make its drift proportional to t), Moran and Hoover [27] modified equations (1.6) as follows:

$$d\tilde{\mathbf{q}}/dt = \mathbf{v}, \qquad d\mathbf{v}/dt = \mathbf{E} - \zeta\mathbf{v}, \tag{1.9}$$

where $\zeta = \langle \mathbf{E}, \mathbf{v}\rangle / \|\mathbf{v}\|^2$. The friction term $\zeta\mathbf{v}$ is called the Gaussian thermostat, it ensures that $\|\mathbf{v}\| = \text{const}$ at all times; again we will assume that $\|\mathbf{v}\| = 1$. We also assume that the field is weak, i.e. $\mathbf{E} = (\varepsilon, 0)$ for a small $\varepsilon > 0$.

The resulting dynamics is now truly periodic – it can be projected onto the domain $\mathcal{D}$ with periodic boundary conditions, then we obtain a system with the same phase space $\Omega = \mathcal{D} \times \mathbb{S}^1$ and the same collision space $\mathcal{M}$ as for the billiards discussed earlier. We denote by Φ_ε^t the resulting flow on Ω

and by $\mathcal{F}_\varepsilon$ the resulting collision map on $\mathcal{M}$. Also let $\tau_\varepsilon(X)$ denote the time of the first collision of the trajectory starting at $X \in \mathcal{M}$. And we denote by $\mathbf{\Delta}_\varepsilon(X) = \tilde{\mathbf{q}}_1 - \tilde{\mathbf{q}}_0$ the displacement of the particle moving in the infinite domain $\tilde{\mathcal{D}}$ before its next collision at $\partial\tilde{\mathcal{D}}$.

Theorem 4 ([18, 19])**.** *Let $\tilde{\mathcal{D}}$ have finite horizon and ε be sufficiently small. Then $\mathcal{F}_\varepsilon$ is a hyperbolic map; it preserves a Sinai-Ruelle-Bowen (SRB) measure (a steady state) ν_ε, which is ergodic and mixing. It is singular but positive on open sets. The flow Φ_ε^t also preserves an SRB measure μ_ε on Ω, which is ergodic, mixing, and positive on open sets. The electrical current*

$$\mathbf{J} = \lim_{t\to\infty} \tilde{\mathbf{q}}(t)/t = \mu_\varepsilon(\mathbf{v}) = \nu_\varepsilon(\mathbf{\Delta}_\varepsilon)/\bar{\tau}_\varepsilon$$

is well defined; here $\bar{\tau}_\varepsilon = \nu_\varepsilon(\tau_\varepsilon)$ is the mean free path for which we have $\bar{\tau}_\varepsilon = \bar{\tau} + \mathcal{O}(\varepsilon)$. We have

$$\mathbf{J} = \tfrac{1}{2\bar{\tau}}\,\mathbf{D}\mathbf{E} + o(\varepsilon), \tag{1.10}$$

where $\mathbf{D}$ is the diffusion matrix of Theorem 1. We also have the following weak convergence, as $t \to \infty$:

$$\frac{\tilde{\mathbf{q}}(t) - \mathbf{J}t}{\sqrt{t}} \Rightarrow \mathcal{N}(0, \mathbf{D}_\varepsilon^*),$$

where $\mathbf{D}_\varepsilon^*$ is the corresponding diffusion matrix *satisfying*

$$\mathbf{D}_\varepsilon^* = \bar{\tau}^{-1}\mathbf{D} + o(1). \tag{1.11}$$

In physical terms, equation (1.10) can be regarded [18, 19] as classical *Ohm's law*: the electrical current $\mathbf{J}$ is proportional to the voltage $\mathbf{E}$ (to the leading order). The fact that the electrical conductivity, i.e. $\frac{1}{2\bar{\tau}}\,\mathbf{D}$ in (1.10), is proportional to the diffusion matrix $\mathbf{D}$ is known as *Einstein relation*.

If the horizon is not finite, then there are infinite corridors between scatterers where the electrons move without collisions. Due to this ballistic motion, the current and diffusion become abnormal in the following exact sense:

Theorem 5 ([15])**.** *Let $\tilde{\mathcal{D}}$ have infinite horizon. Assume that the force $\mathbf{E} = (\varepsilon, 0)$ is not parallel to any of the infinite corridors and ε is sufficiently small. Then $\mathcal{F}_\varepsilon$ is a hyperbolic map; it preserves an SRB measure (steady state) ν_ε, which is ergodic, mixing, and positive on open sets. The flow Φ_ε^t also preserves an SRB measure μ_ε on Ω, which is ergodic, mixing, and positive on open sets. The electrical current*

$$\mathbf{J} = \lim_{t\to\infty} \tilde{\mathbf{q}}(t)/t = \mu_\varepsilon(\mathbf{v}) = \nu_\varepsilon(\mathbf{\Delta}_\varepsilon)/\bar{\tau}_\varepsilon \tag{1.12}$$

is well defined; here $\bar{\tau}_\varepsilon = \nu_\varepsilon(\tau_\varepsilon)$ is the mean free path for which we have $\bar{\tau}_\varepsilon = \bar{\tau} + \mathcal{O}(\varepsilon^a)$ for some $a > 0$. We have

$$\mathbf{J} = \tfrac{1}{2\bar{\tau}}\,|\log\varepsilon|\,\mathbf{D}_\infty\mathbf{E} + \mathcal{O}(\varepsilon) \tag{1.13}$$

where $\mathbf{D}_\infty$ *is the superdiffusion matrix of Theorem* 2. *We also have the following weak convergence, as* $t \to \infty$*:*

$$\frac{\tilde{\mathbf{q}}(t) - \mathbf{J}t}{\sqrt{t}} \Rightarrow \mathcal{N}(0, \mathbf{D}^*_\varepsilon), \tag{1.14}$$

where $\mathbf{D}^*_\varepsilon$ *is the corresponding* diffusion matrix *satisfying*

$$\mathbf{D}^*_\varepsilon = \bar{\tau}^{-1} |\log \varepsilon| \, \mathbf{D}_\infty + \mathcal{O}(1). \tag{1.15}$$

Observe that now the current becomes proportional to $\varepsilon|\log\varepsilon|$, rather than ε, i.e. Ohm's law fails in this regime. This mathematical fact may be related to the physical phenomenon of 'superconductivity'. At low temperatures (near absolute zero), ions tend to form an almost perfect crystal structure with long corridors in between resembling our infinite horizon model. Thus the electron tends to travel fast and one observes superconductivity.

On the other hand, at normal temperatures, ions are somewhat agitated, their configuration is more randomized, which creates an effect of finite horizon. It slows the electron down and one observes a normal current.

To summarize, the Gaussian thermostatted dynamics (1.9) allows us to obtain an adequate description of the ordinary electrical current when the horizon is finite (Theorem 4). It also can be related to superconductivity in the infinite horizon case (Theorem 5).

However, the Gaussian thermostat may be criticized as an unrealistic and artificial device – it acts on the particle all the time, even during the 'free flights' between collisions (thus violating Newton's law (1.6)). It is perhaps more reasonable to allow the electron move freely (and accelerate naturally) between collisions, but remove the excess of its energy when it collides with heavy immovable ions. In other words, the thermostat should be placed on the boundaries of the ions (i.e. at the walls of $\tilde{\mathcal{D}}$).

Our objectives. In this paper we propose a dynamics of that kind. Our electrons move freely, according to Newton's law (1.6), so that their kinetic energy may grow. But at every collision with ions the speed of the electron is reset so that it remains bounded. In fact if the electron was transported back to the original cell after every collision, then its total energy would remain fixed. Reflections off the wall $\partial\tilde{\mathcal{D}}$ are kept specular, i.e. the angle of incidence is still equal to the angle of reflection.

Our ultimate goal is to show that all the conclusions of Theorems 4 and 5 remain valid in this new context. Thus we present a more realistic version of the Lorentz gas in a constant external field than the Gaussian thermostatted model studied in [18, 19, 13]. Our dynamics with thermostatted walls constitutes the physical novelty of the paper.

Besides being physically more realistic, our dynamics also has mathematical advantages compared to the Gaussian thermostat. Namely, the Galton board can be regarded as a slow-fast system where the kinetic energy is a slow variable while particle's position in $\mathcal{D}$ and its velocity direction are fast variables. The velocity vector of the Gaussian thermostatted model (1.9) is simply obtained by projecting the velocity vector (1.6) onto the surface of

constant kinetic energy; therefore the Gaussian thermostatted model represents the so called *frozen system* (its slow variable is rigidly fixed, i.e. frozen). Frozen systems may provide good approximations to slow-fast systems, and such an approximation played a fundamental role in our studies of the Galton board with finite horizon [13]. However, in the infinite horizon case this approximation turns out to be poor, because during long free flights in infinite corridors small errors accumulate and grow too much. Here we reset the energy only at the time of collisions, so our new model provides a much better approximation to the Galton board dynamics.

Our mathematical constructions and arguments are also unusual in many ways. In all the previous studies [18, 9, 11, 13, 15] of billiard-like particles moving under external forces, the dynamics was time-reversible, or at least invertible. That is, the flow Φ^t was well defined for all $-\infty < t < \infty$, and the collision map $\mathcal{F}$ was invertible, i.e. $\mathcal{F}^{-1}$ existed. Thus the Lyapunov exponents could be computed and the dynamics could be (and usually were) hyperbolic. Then all the mathematical tools developed for hyperbolic systems (Markov partitions, Young tower construction, Coupling method, etc.) could be applied with a remarkable success resulting in Theorems 3–5.

Our model is different. The energy of the electron is 'reset' at every collision to a fixed level, thus it 'forgets' its past. As a result, its past trajectory cannot be uniquely recovered from its present state. The dynamics ceases to be invertible – some phase points have multiple preimages, while others have none. Lyapunov exponents can only be computed under forward iterations (but not under backward iterations), and the system cannot be hyperbolic in the ordinary sense.

More precisely, our collision map $\mathcal{F}\colon \mathcal{M} \to \mathcal{M}$ will be piecewise smooth in the sense that $\mathcal{M}$ will be a finite union of subdomains, $\mathcal{M} = \cup_i \mathcal{M}_i^+$, on each of which $\mathcal{F}$ will be smooth and diffeomorphic, but the images $\mathcal{F}(\mathcal{M}_i^+)$ and $\mathcal{F}(\mathcal{M}_j^+)$ will overlap for some $i \neq j$. Furthermore, their union $\cup_i \mathcal{F}(\mathcal{M}_i^+)$ will not cover $\mathcal{M}$ entirely – there will be open gaps (or 'cracks') in between. In the gaps, $\mathcal{F}^{-1}$ will not be defined, thus there will be no unstable manifolds. At points in the overlapping regions, $\mathcal{F}^{-1}$ will be multiply defined, thus unstable manifolds will not be unique.

Dynamically, our map $\mathcal{F}$ resembles a hyperbolic map with singularities, in particular it has stable and unstable cones (though defined only under forward iterations). Stable manifolds are well defined, but unstable manifolds may not exist or may not be unique. In a way, our map $\mathcal{F}$ can be compared to non-invertible expanding maps where only the future evolution is uniquely defined.

In other words, our map $\mathcal{F}$ does not belong to any standard class of chaotic dynamical systems, it is somewhere 'between' invertible hyperbolic maps and non-invertible expanding maps (though much closer to the former than to the latter). Such maps are interesting from a purely dynamical point of view, but very little is known about them.

Many examples of such maps can be easily constructed. For one, let $F_0 \colon \mathbb{T} \to \mathbb{T}$ be a hyperbolic toral automorphism of a unit 2-torus; let $\mathbb{T} = M_1 \cup \cdots M_k$ be a finite partition of $\mathbb{T}$ into domains with piecewise smooth boundaries, and let $F_1 \colon \mathbb{T} \to \mathbb{T}$ be a map that is smooth on each M_i and its restriction to M_i is a C^2-perturbation of the identity map on M_i. Then $F = F_0 \circ F_1$ is a map of the sort described above – it has strong hyperbolic features, but the images of M_i may overlap and/or leave uncovered gaps. Despite the simplicity of such examples, they were rarely studied in the past.

In recent papers [2, 3], Baladi and Gouëzel considered non-invertible maps with stable and unstable cones and bounded derivatives; they used operator techniques to derive the existence and 'finitude' of physical invariant measures. A particular countable-to-one map with stable and unstable cones was investigated in [16], where natural extensions were used to cope with non-invertibility. In our current model, the derivatives are unbounded, so we have to use methods different from [2, 3]. We develop a general approach to the construction of SRB-like ("physical") invariant measures which works for countable-to-one maps and does not require strong *a priori* bounds on the probabilities of particular inverse branches which were needed in [16]. So we develop alternative methods that hopefully will be useful for future similar studies. Our ideas are similar to those developed in [1] in the context of partially hyperbolic diffeomorphisms.

We also note that [2, 3] and [16] deal with statistical properties of individual systems, while we study a continuous family of systems. Its dependence on the parameter ε plays an important role. The question of smoothness of SRB measures for piecewise hyperbolic systems is far from being settled, see discussions in [4, 28]. Our model provides a new example where transport theory works (i.e., Ohm's law and the Einstein relation hold), so we hope it could be useful for the development of a more general theory.

In the next section we precisely describe our dynamics with 'thermostatted walls' and state our main results.

2. The model and main results

We define the dynamics in $\mathcal{D}$ as follows. First we fix an external field $\mathbf{E} = (\varepsilon, 0)$; here $\varepsilon > 0$ is a small constant. In our dynamics the particle has a fixed total energy so that $\|\mathbf{v}\|^2 - 2\varepsilon x = 1$, cf. (1.8), and moves under the field $\mathbf{E}$ between collisions.

More precisely, let $\mathbf{q} = (x, y) \in \partial\mathcal{D}$ be a point where the particle collides with a scatterer and $\mathbf{v}$ denotes the outgoing velocity vector. Since the total energy is fixed, we have

$$v = \|\mathbf{v}\| = \sqrt{1 + 2\varepsilon x}. \tag{2.1}$$

Leaving the scatterer, the particle moves under the external field $\mathbf{E}$ according to the standard equations

$$d\mathbf{q}/dt = \mathbf{v}, \qquad d\mathbf{v}/dt = \mathbf{E}, \tag{2.2}$$

until it collides with another scatterer. The motion between collisions is smooth, so that it is better visualized if we allow the particle move on the unbounded domain $\tilde{\mathcal{D}}$. In particular, if the particle crosses the border of the fundamental cell $\mathcal{K}$, it leaves $\mathcal{D}$ and enters another domain $\mathcal{D}_i$, etc. In this way the x-coordinate of the moving particle changes continuously, and so does its speed, according to (2.1). But when the particle collides with a scatterer in $\mathbb{R}^2$, i.e. when its hits $\partial\tilde{\mathcal{D}}$, it is instantaneously projected back onto $\mathcal{D}$, under the natural projection $\tilde{\pi}$. As we apply the projection $\tilde{\pi}$, the x-coordinate of the particle can change, thus we need to adjust its speed, too, in order to keep the total energy fixed, according to (2.1); when adjusting the speed, we keep the direction of the velocity vector unchanged. Then the motion continues.

In this way our obstacles act not only as scatterers but also as 'heat baths' or 'thermostats', which remove the excess of the particle's kinetic energy and keep it bounded (but not constant).

Remark. It is tempting to define a thermostat simply by resetting the kinetic energy (i.e., the speed) of the particle to a constant value after every collision. We will show that such dynamics would cause formidable complications, though. In fact the only way to keep the features of the model tractable is to reset the *total* energy in the above sense; see Appendix.

Remark. Our dynamics clearly depends on the choice of the fundamental domain, which is far from unique, but this choice does not affect our main results. For example, if $\mathcal{K} = [0,1] \times [0,1]$ is a unit square, then one can alternatively define $\mathcal{K} = [a, 1+a] \times [b, 1+b]$ for any $a, b > 0$. In that case the trajectories of our particle would change by $\mathcal{O}(\varepsilon^2)$, which is too small to affect our results. (Loosely speaking, our dynamics is a $\mathcal{O}(\varepsilon)$-perturbation of the field-free billiard system, and further changes of order $\mathcal{O}(\varepsilon^2)$ are negligible.) One can also combine several copies of $\mathcal{K}$ into a bigger fundamental domain. For example, if $\mathcal{K} = [0,1] \times [0,1]$, then one can define $\mathcal{K} = [0,m] \times [0,n]$ for any positive integers $m, n \geq 1$. The resulting changes in the dynamics are not essential either, as we will explain at the end of Section 5.

It is important to estimate how far the particle can travel between collisions and thus how much its speed can change. In the finite horizon case, the free path is bounded, hence the speed remains $1 + \mathcal{O}(\varepsilon)$. In the infinite horizon case, we assume that the corridors between scatterers are not parallel to the field $\mathbf{E}$.

Lemma 2.1. *The longest free path (i.e., the length of the trajectory segment between consecutive collisions) is* $\mathcal{O}(\varepsilon^{-1/2})$. *Thus the speed of the particle between collisions remains* $1 + \mathcal{O}(\varepsilon^{1/2})$. *At the same time, its speed right after each collision is* $1 + \mathcal{O}(\varepsilon)$, *according to* (2.1).

Proof. Between collisions the particle moves along parabolas. The proof requires elementary calculations which we leave to the reader. □

We see that the magnitude of the velocity vector remains close to one (and is completely determined by the x-coordinate of the particle). Hence the velocity vector is specified uniquely by its direction, the fact we use below.

We can define the collision space by

$$\mathcal{M} = \big\{(\mathbf{q}, \mathbf{v})\colon \mathbf{q} = (x, y) \in \partial\mathcal{D},\ \|\mathbf{v}\| = \sqrt{1 + 2\varepsilon x},\ \mathbf{v} \text{ points inside } \mathcal{D}\big\}.$$

We will use standard coordinates r, φ on $\mathcal{M}$, where r denotes the arclength parameter on the boundary $\partial\mathcal{D}$ and φ the angle between the outgoing velocity vector $\mathbf{v}$ and the normal vector to $\partial\mathcal{D}$ pointing inside $\mathcal{D}$; thus $\varphi \in [-\pi/2, \pi/2]$. We orient the coordinates so that r increases when one traverses $\partial\mathcal{D}$ in such a way that the domain $\mathcal{D}$ remains on the left hand side, and the value $\varphi = \pi/2$ corresponds to direction of growth of r; see Figure 3.

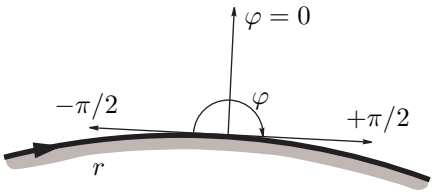

FIGURE 3. Orientation of r and φ.

Note that the domain of the variables r, φ does not depend on ε. In the coordinates r, φ the space $\mathcal{M}$ becomes a rectangle

$$\mathcal{M} = [0, L] \times [-\pi/2, \pi/2], \qquad \text{where } L = \text{length}(\partial\mathcal{D})$$

(topologically, it is rather a union of cylinders, as r is a cyclic coordinate on each scatterer). Thus we regard $\mathcal{M}$ as independent of ε, so the collision map $\mathcal{F}_\varepsilon\colon \mathcal{M} \to \mathcal{M}$ acts on the same space for all small ε. Note that $\mathcal{F}_0 = \mathcal{F}$ is the billiard collision map discussed earlier. In a sense, $\mathcal{F}_\varepsilon$ is a small perturbation of $\mathcal{F}_0$, see below.

Next, for every point $X \in \mathcal{M}$ we denote by $\tau_\varepsilon(X)$ the time it moves until the next collision with $\partial\tilde{\mathcal{D}}$. Thus we obtain a suspension flow Φ_ε^t over the map $\mathcal{F}_\varepsilon$ under the function τ_ε. We denote by

$$\Omega = \{(X, t)\colon X \in \mathcal{M},\ \ 0 \le t \le \tau_\varepsilon(X)\}$$

the phase space of the suspension flow. Note that now our trajectories are parameterized by t.

Lastly we lift our dynamics from the compact domain $\mathcal{D}$ with periodic boundary conditions to the unbounded table $\tilde{\mathcal{D}}$. This can be done naturally as follows. Recall that the particle starts at a point $\mathbf{q} = (x, y)$ on a scatterer in $\mathcal{D}$ with initial speed $v_0 = \sqrt{1 + 2\varepsilon x}$. It moves according to (2.2) until its trajectory lands at a point $\tilde{\mathbf{q}}_1 = (x_1, y_1)$ on another scatterer in some domain $\mathcal{D}^{(1)} \subset \mathbb{R}^2$. Before the collision, its speed is $v_1^- = \sqrt{1 + 2\varepsilon x_1}$. After

the collision its speed is reset to $v_1^+ = \sqrt{1 + 2\varepsilon(x_1 - Z_x^{(1)})}$, where $Z_x^{(1)}$ denotes the displacement, in the x direction, between the domains $\mathcal{D}$ and $\mathcal{D}^{(1)}$ (this means that $\mathcal{D}^{(1)}$ is obtained from $\mathcal{D}$ by translation along vector $\mathbf{Z}^{(1)}$ whose x-coordinate is denoted by $Z_x^{(1)}$).

Instead of translating the particle's position from $\tilde{\mathbf{q}}_1 \in \mathcal{D}^{(1)}$ to $\tilde{\mathbf{q}}_1 - \mathbf{Z}^{(1)} \in \mathcal{D}^{(0)}$, as we did before, we now let it continue its motion in the unbounded domain $\tilde{\mathcal{D}}$, i.e. its trajectory will run from $\tilde{\mathbf{q}}_1$, with initial speed v_1^+, until it hits a scatterer in another domain $\mathcal{D}^{(2)} \subset \mathbb{R}^2$, and we denote the collision point by $\tilde{\mathbf{q}}_2 = (x_2, y_2)$. By that time its speed is $v_2^- = \sqrt{1 + 2\varepsilon(x_2 - Z_x^{(1)})}$, but we reset it to $v_2^+ = \sqrt{1 + 2\varepsilon(x_2 - Z_x^{(2)})}$, where $Z_x^{(2)}$ is the displacement, in the x direction, between the domains $\mathcal{D}$ and $\mathcal{D}^{(2)}$. Then the particle runs further, from the point $\tilde{\mathbf{q}}_2$ until its next collision with $\partial\tilde{\mathcal{D}}$, etc.

The so defined motion on $\tilde{\mathcal{D}}$ is a natural lift to the plane $\mathbb{R}^2$ of the motion on $\mathcal{D}$ constructed before. Thus for each initial state $(\mathbf{q}, \mathbf{v}) \in \mathcal{M}$ we get a sequence $\tilde{\mathbf{q}}_n \in \mathbb{R}^2$ of collision points and a continuous trajectory $\tilde{\mathbf{q}}(t)$ of the particle, where the time variable t corresponds to our suspension flow Φ_ε^t. We also have velocity $\mathbf{v} = d\tilde{\mathbf{q}}(t)/dt$. We denote by $\boldsymbol{\Delta}_\varepsilon = (\Delta_{\varepsilon,x}, \Delta_{\varepsilon,y}) = \tilde{\mathbf{q}}_1 - \mathbf{q}$ the displacement vector between consecutive collisions; it is a function on $\mathcal{M}$.

Now the particle's position $\tilde{\mathbf{q}}(t) \in \mathbb{R}^2$ represents the electrical current, and we can state our main results. The first one is an analogue of Theorem 4:

Theorem 6. *Let $\tilde{\mathcal{D}}$ have finite horizon and ε be sufficiently small. Then $\mathcal{F}_\varepsilon$ is a hyperbolic map; it preserves a unique Sinai-Ruelle-Bowen (SRB) measure (a steady state) ν_ε, which is ergodic and mixing and enjoys exponential decay of correlations. The flow Φ_ε^t also preserves a unique SRB measure μ_ε on Ω, which is ergodic and mixing. The electrical current*

$$\mathbf{J} = \lim_{t\to\infty} \tilde{\mathbf{q}}(t)/t = \mu_\varepsilon(\mathbf{v}) = \nu_\varepsilon(\boldsymbol{\Delta}_\varepsilon)/\bar{\tau}_\varepsilon \tag{2.3}$$

is well defined; here $\bar{\tau}_\varepsilon = \nu_\varepsilon(\tau_\varepsilon)$ is the mean free path for which we have $\bar{\tau}_\varepsilon = \bar{\tau} + \mathcal{O}(\varepsilon^a)$ for some $a > 0$. We have

$$\mathbf{J} = \tfrac{1}{2\bar{\tau}}\,\mathbf{D}\mathbf{E} + o(\varepsilon), \tag{2.4}$$

where $\mathbf{D}$ is the diffusion matrix of Theorem 1. We also have the following weak convergence, as $t \to \infty$:

$$\frac{\tilde{\mathbf{q}}(t) - \mathbf{J}t}{\sqrt{t}} \Rightarrow \mathcal{N}(0, \mathbf{D}_\varepsilon^*), \tag{2.5}$$

where $\mathbf{D}_\varepsilon^*$ is the corresponding diffusion matrix *satisfying*

$$\mathbf{D}_\varepsilon^* = \bar{\tau}^{-1}\mathbf{D} + o(1). \tag{2.6}$$

The second main result is an analogue of Theorem 5:

Theorem 7. *Let $\tilde{\mathcal{D}}$ have infinite horizon. Assume that the force $\mathbf{E} = (\varepsilon, 0)$ is not parallel to any of the infinite corridors and ε is sufficiently small. Then $\mathcal{F}_\varepsilon$ is a hyperbolic map; it preserves a unique SRB measure (steady state)*

ν_ε, which is ergodic and mixing and enjoys exponential decay of correlations. The flow Φ_ε^t also preserves a unique SRB measure μ_ε on Ω, which is ergodic and mixing. The electrical current

$$\mathbf{J} = \lim_{t\to\infty} \tilde{\mathbf{q}}(t)/t = \mu_\varepsilon(\mathbf{v}) = \nu_\varepsilon(\mathbf{\Delta}_\varepsilon)/\bar{\tau}_\varepsilon \tag{2.7}$$

is well defined; here $\bar{\tau}_\varepsilon = \nu_\varepsilon(\tau_\varepsilon)$ is the mean free path for which we have $\bar{\tau}_\varepsilon = \bar{\tau} + \mathcal{O}(\varepsilon^a)$ for some $a > 0$. We have

$$\mathbf{J} = \tfrac{1}{2\bar{\tau}} \,|\log\varepsilon|\, \mathbf{D}_\infty \mathbf{E} + \mathcal{O}(\varepsilon) \tag{2.8}$$

where $\mathbf{D}_\infty$ is the superdiffusion matrix of Theorem 2. We also have the following weak convergence, as $t \to \infty$:

$$\frac{\tilde{\mathbf{q}}(t) - \mathbf{J}t}{\sqrt{t}} \Rightarrow \mathcal{N}(0, \mathbf{D}_\varepsilon^*), \tag{2.9}$$

where $\mathbf{D}_\varepsilon^*$ is the corresponding diffusion matrix *satisfying*

$$\mathbf{D}_\varepsilon^* = \bar{\tau}^{-1} |\log\varepsilon|\, \mathbf{D}_\infty + \mathcal{O}(1). \tag{2.10}$$

We note that the invariant measures in Theorems 6 and 7 are not positive on open sets (unlike SRB measures for the Gaussian thermostatted dynamics). We do not know if their support (i.e., the intersection of all closed sets of full measure) has a positive Lebesgue measure or not; we return to that issue in Section 8.

We will prove Theorems 6 and 7 in parallel. Our arguments follow a general scheme developed in [15, 18] for the Gaussian thermostatted Lorentz gases, but we have to modify many steps of that scheme to deal with the non-invertibility of our dynamics.

In Section 3–5 we show that the map $\mathcal{F}_\varepsilon$ is a small (in a certain sense) perturbation of the billiard map $\mathcal{F}_0$, it has stable and unstable cones and estimate the sizes of overlaps and gaps in $\mathcal{M}$. Our technical analysis here is essentially different from that in all the previous studies [9, 15, 18], so we give a detailed presentation.

In Section 6 we describe the singularities of $\mathcal{F}_\varepsilon$ and in Section 7 build up our main tools – standard pairs and families – and prove the key growth lemma. Our arguments are similar to those of [15], so we only present them briefly. But the construction of the SRB measure ν_ε in Section 8 is quite novel and is presented in full.

All the formulas in Theorems 6 and 7 are then derived in Sections 9 and 10, based on a substantial modification of the arguments of [15].

3. Perturbative analysis

Here we derive formulas for the differential of our collision map $\mathcal{F}_\varepsilon$ and show that it is a small perturbation of the billiard map $\mathcal{F}_0$.

Let $X = (r, \varphi) \in \mathcal{M}$ be a phase point and $X_1 = \mathcal{F}_\varepsilon(X) = (r_1, \varphi_1)$ denote its image. Denote by $(x, y) \in \partial\mathcal{D}$ and $(x_1, y_1) \in \partial\mathcal{D}$ the coordinates of the boundary points corresponding to r and r_1. Denote by ω and ω_1 the

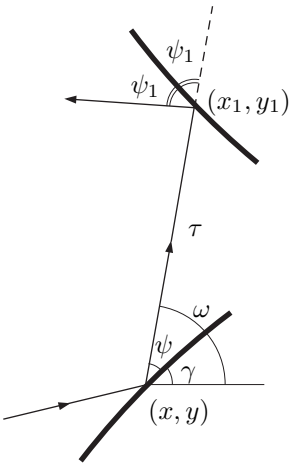

FIGURE 4. Action of the map in coordinates.

angles made by the outgoing velocity vector at the point X and the incoming velocity vector at the point X_1, respectively, with the x axis; see Fig. 4. Here and in what follows we use notation of [17, Section 2.11], where a similar analysis was done for the billiard dynamics. Our aim is to express dr_1 and $d\varphi_1$ in terms of dr and $d\varphi$, and we use differentials of other variables in the process.

We denote by γ and γ_1 the slopes of the tangents to $\partial\mathcal{D}$ at the points r and r_1, respectively. We also denote

$$\psi = \pi/2 - \varphi \qquad \text{and} \qquad \psi_1 = \pi/2 - \varphi_1.$$

Observe that

$$\omega = \gamma + \psi \qquad \text{and} \qquad \omega_1 = \gamma_1 - \psi_1. \tag{3.1}$$

Our trajectory curves under the action of the field $\mathbf{E}$, and so in general $\omega_1 \neq \omega$. We put $\delta = \omega_1 - \omega$.

Let $\mathcal{K} > 0$ and $\mathcal{K}_1 > 0$ denote the curvature of $\partial\mathcal{D}$ at the points r and r_1, respectively. Note that, in terms of differentials,

$$d\gamma = -\mathcal{K}\, dr \qquad \text{and} \qquad d\gamma_1 = -\mathcal{K}_1\, dr_1. \tag{3.2}$$

Also note that

$$dx = \cos\gamma\, dr \qquad \text{and} \qquad dy = \sin\gamma\, dr,$$

as well as

$$dx_1 = \cos\gamma_1\, dr_1 \qquad \text{and} \qquad dy_1 = \sin\gamma_1\, dr_1.$$

Let v denote the speed of the particle when it departs from the point (x, y), and v_1 denote its speed right before it arrives at (x_1, y_1). Of course,

the conservation of the total energy implies

$$v^2 - 2\varepsilon x = v_1^2 - 2\varepsilon x_1 = 1.$$

In particular,

$$v\,dv = \varepsilon \cos\gamma\, dr. \tag{3.3}$$

Now solving the equations (2.2) we obtain

$$v_1 \cos\omega_1 = v\cos\omega + \varepsilon\tau \qquad \text{and} \qquad v_1 \sin\omega_1 = v\sin\omega \tag{3.4}$$

and

$$x_1 = x + v\tau\cos\omega + \tfrac{1}{2}\varepsilon\tau^2 \qquad \text{and} \qquad y_1 = y + v\tau\sin\omega, \tag{3.5}$$

where τ is the travel time between the points (x, y) and (x_1, y_1). Equations (3.4) can be rewritten as

$$v_1 = v\cos\delta + \varepsilon\tau\cos\omega_1 \qquad \text{and} \qquad v\sin\delta + \varepsilon\tau\sin\omega_1 = 0. \tag{3.6}$$

Differentiating (3.5) yields

$$\begin{aligned} \cos\gamma_1\, dr_1 &= \cos\gamma\, dr + v\cos\omega\, d\tau - v\tau\sin\omega\, d\omega + \tau\cos\omega\, dv + \varepsilon\tau\, d\tau \\ \sin\gamma_1\, dr_1 &= \sin\gamma\, dr + v\sin\omega\, d\tau + v\tau\cos\omega\, d\omega + \tau\sin\omega\, dv. \end{aligned} \tag{3.7}$$

Using (3.4) we can rewrite (3.7) as

$$\begin{aligned} \cos\gamma_1\, dr_1 &= \cos\gamma\, dr + v_1\cos\omega_1\, d\tau - v\tau\sin\omega\, d\omega + \tau\cos\omega\, dv \\ \sin\gamma_1\, dr_1 &= \sin\gamma\, dr + v_1\sin\omega_1\, d\tau + v\tau\cos\omega\, d\omega + \tau\sin\omega\, dv. \end{aligned} \tag{3.8}$$

Next we eliminate $d\tau$ from (3.8) using (3.1) and arrive at

$$\sin\psi_1\, dr_1 + \sin(\psi + \delta)\, dr - v\tau\cos\delta\, d\omega + \tau\sin\delta\, dv = 0. \tag{3.9}$$

Similarly, eliminating $d\omega$ from (3.7) gives

$$\cos(\psi_1 + \delta)\, dr_1 = \cos\psi\, dr + (v + \varepsilon\tau\cos\omega)\, d\tau + \tau\, dv. \tag{3.10}$$

Now the second equation in (3.6) implies

$$v + \varepsilon\tau\cos\omega = -\frac{\varepsilon\tau\cos\delta\sin\omega}{\sin\delta} \tag{3.11}$$

thus (3.10) can be written as

$$\sin\delta\cos(\psi_1 + \delta)\, dr_1 = \sin\delta\cos\psi\, dr - \varepsilon\tau\cos\delta\sin\omega\, d\tau + \tau\sin\delta\, dv. \tag{3.12}$$

Differentiating the second equation in (3.6) yields

$$v\cos\delta(d\omega_1 - d\omega) + \sin\delta\, dv + \varepsilon\sin\omega_1\, d\tau + \varepsilon\tau\cos\omega_1\, d\omega_1 = 0$$

and combining this with the first equation in (3.6) gives

$$v_1\, d\omega_1 - v\cos\delta\, d\omega + \sin\delta\, dv + \varepsilon\sin\omega_1\, d\tau = 0. \tag{3.13}$$

Now eliminating $d\tau$ from (3.12) and (3.13) gives

$$\begin{aligned} &\sin\delta\cos\psi\sin\omega_1\, dr - \sin\delta\cos(\psi_1 + \delta)\sin\omega_1\, dr_1 \\ &\quad + v_1\tau\cos\delta\sin\omega\, d\omega_1 - v\tau\cos^2\delta\sin\omega\, d\omega \\ &\quad + \tau\sin\delta\sin\omega_1\, dv + \tau\sin\delta\cos\delta\sin\omega\, dv = 0. \end{aligned} \tag{3.14}$$

Recall (3.3) and observe that

$$d\omega = -\mathcal{K}\, dr + d\psi \qquad \text{and} \qquad d\omega_1 = -\mathcal{K}_1\, dr_1 - d\psi_1$$

thus we can solve the two equations (3.9) and (3.14) for dr_1 and $d\psi_1$. We record their solutions by using the standard variables $\varphi = \pi/2 - \psi$ and $\varphi_1 = \pi/2 - \psi_1$:

$$-\cos\varphi_1\, dr_1 = [\mathcal{K}v\tau\cos\delta + \cos(\varphi - \delta)]dr + \tau\sin\delta\, dv + v\tau\cos\delta\, d\varphi \quad (3.15)$$

and

$$\begin{aligned} -v_1\tau\, d\varphi_1 = {} & \big[\mathcal{K}v\tau\cos\delta + \sin\delta\sin\varphi(1+\tan\delta\cot\omega)\big]dr \\ & + \tau\sin\delta\big[1+\sin\omega_1/(\cos\delta\sin\omega)\big]dv + v\tau\cos\delta\, d\varphi \\ & - \big[\mathcal{K}_1 v_1\tau + \sin\delta\sin(\varphi_1-\delta)(1+\tan\delta\cot\omega)\big]dr_1, \end{aligned} \quad (3.16)$$

where

$$dv = (\varepsilon\cos\gamma/v)dr \quad (3.17)$$

according to (3.3). Equations (3.15)–(3.16) represent the derivative of the map $\mathcal{F}_\varepsilon$ in the (r,φ) coordinates.

When $\varepsilon = 0$, our system reduces to the usual billiard dynamics in which $v = v_1 = 1$ and $\delta = 0$, and we recover the derivative of the billiard collision map, in the $r\varphi$ coordinates (see (2.26) in [17]):

$$D\mathcal{F}_0 = \frac{-1}{\cos\varphi_1}\begin{bmatrix} \tau\mathcal{K}+\cos\varphi & \tau \\ \tau\mathcal{K}\mathcal{K}_1 + \mathcal{K}\cos\varphi_1 + \mathcal{K}_1\cos\varphi & \tau\mathcal{K}_1 + \cos\varphi_1 \end{bmatrix}. \quad (3.18)$$

Next we estimate corrections due to the external field $\mathbf{E}$. First note that $\varepsilon\tau = \mathcal{O}(\varepsilon^{1/2})$ is small, by Lemma 2.1. Then we note that

$$v = 1 + \mathcal{O}(\varepsilon) \qquad \text{and} \qquad v_1 = 1 + \mathcal{O}(\varepsilon\tau)$$

and it follows from the second equation in (3.6) that

$$\sin\delta \sim -\frac{\varepsilon\tau\sin\omega}{1+\mathcal{O}(\varepsilon\tau)} \quad (3.19)$$

thus all the $\cot\omega$ factors in (3.16) will be neutralized by $\sin\delta$.

Now a direct analysis shows that the derivative of $\mathcal{F}_\varepsilon$ satisfies

$$D\mathcal{F}_\varepsilon = D\mathcal{F}_0 + \frac{1}{\cos\varphi_1}\mathcal{O}_{2\times2}(\varepsilon\tau), \quad (3.20)$$

where $\mathcal{O}_{2\times2}(\varepsilon\tau)$ denotes a matrix 2×2 whose entries are $\mathcal{O}(\varepsilon\tau)$ uniformly over $\mathcal{M}$.

We note that (3.20) does not really mean that $\mathcal{F}_\varepsilon$ is C^1-close to $\mathcal{F}_0$. What it means is that the derivative of the map $\mathcal{F}_\varepsilon$ at a point (r,φ), whose image is (r_1,φ_1), is close to the derivative of a (hypothetical) billiard map that takes (r,φ) to the same image (r_1,φ_1). But the real billiard map $\mathcal{F}_0$ on $\mathcal{D}$ may take (r,φ) to a quite different point, which may even be on a different scatterer. Still, the closeness in the sense of (3.20) has important implications.

4. 'Cone' hyperbolicity

Here we establish certain hyperbolic properties of the map $\mathcal{F}_\varepsilon$. Similar maps were studied recently by Baladi and Gouëzel [2, 3] who described them by the term *cone hyperbolicity*.

Recall that the billiard map $\mathcal{F}_0$ is hyperbolic [17]. Its unstable vectors $dX = (dr, d\varphi)$ can be defined by

$$0 < C_1 \le d\varphi/dr \le C_2 < \infty, \tag{4.1}$$

where $C_1 < C_2$ are some constants. The expansion factor satisfies

$$\|D\mathcal{F}_0(dX)\|_*/\|dX\|_* \ge 1 + a/\cos\varphi_1 \tag{4.2}$$

for some constant $a = a(\mathcal{D}) > 0$, where φ_1 again denotes the reflection angle at $\mathcal{F}(X)$ and $\|dX\|_*$ is an adapted metric. The latter can be defined in various ways, for example (see [17, Section 5.10])

$$\|dX\|_* = |\mathcal{K}\, dr + d\varphi|, \tag{4.3}$$

where $\mathcal{K} > 0$ again denotes the curvature of $\partial\mathcal{D}$ at the given point.

The estimate (3.20) shows that $\mathcal{F}_\varepsilon$ expands the same unstable vectors (4.1), and the expansion factor satisfies (4.2), with a possibly smaller constant $a > 0$. More precisely, the expansion factor of unstable vectors satisfies

$$\frac{(dr_1^2 + d\varphi_1^2)^{1/2}}{(dr^2 + d\varphi^2)^{1/2}} \asymp \frac{dr_1}{dr} \asymp \frac{\tau}{\cos\varphi_1}, \tag{4.4}$$

which for billiards is a standard formula [17, Eq. 4.20]; we use the notation $A \asymp B$ in the sense that $0 < c_1 \le A/B \le c_2 < \infty$ for some constants c_1, c_2 that may depend on $\mathcal{D}$ but not on ε.

Unstable curves are described by functions $\varphi = \varphi(r)$ whose slope is positive and bounded above and below, i.e. unstable curves are increasing in the $r\varphi$ coordinates. Let $W \subset \mathcal{M}$ be an unstable curve and $W_n = \mathcal{F}_\varepsilon^n(W)$ is its image under $\mathcal{F}_\varepsilon^n$ (which is a union of unstable curves). For $X \in W$, we denote by $\mathcal{J}_W\mathcal{F}_\varepsilon(X)$ the Jacobian of $\mathcal{F}_\varepsilon$ restricted to W (i.e., the factor of expansion of W under the map $\mathcal{F}_\varepsilon$) at the point X. We also denote by $\mathcal{J}_{W_1}\mathcal{F}_\varepsilon^{-1}(X_1)$ the Jacobian of the inverse map $W_1 \to W$ at the point $X_1 = \mathcal{F}_\varepsilon(X)$. Next we verify two standard regularity properties for unstable curves.

Lemma 4.1 (Curvature bounds). *Suppose that $|d^2\varphi/dr^2| \le C_0$ at all points $(\varphi, r) \in W$, for some $C_0 > 0$. Then there is a constant $C = C(C_0, \mathcal{D}) > 0$ such that for all $n \ge 1$ we have $|d^2\varphi_n/dr_n^2| \le C$ at all points $(\varphi_n, r_n) \in W_n$.*

Due to this lemma, we can (and will) assume that all our unstable curves have uniformly bounded curvature; this assumption is standard for billiards and their perturbations [9, 17].

Proof. For the billiard maps and their perturbations by external forces (though different from ours) this lemma was proved in [9]. A more direct proof (for the billiard maps only) is given in [12, Equation (B.2)]. The last proof can be adapted to our case if we estimate the corrections to the second order derivatives due to the external field $\mathbf{E}$. In fact, all those corrections are of

order $\mathcal{O}(\varepsilon\tau)$. For example, in billiards $dv/dr = 0$ and in our model $dv/dr = \mathcal{O}(\varepsilon\tau)$ due to (3.17). Differentiating the second equation in (3.6) gives $d\delta = \mathcal{O}(\varepsilon\tau\, dr_1)$. Solving (3.10) for $d\tau$ gives $d\tau = \cos\psi_1\, dr_1 - \cos\psi\, dr + \mathcal{O}(\varepsilon\tau\, dr_1)$, while for the billiard map we have $d\tau = \cos\psi_1\, dr_1 - \cos\psi\, dr$, so the remainder $\mathcal{O}(\varepsilon\tau\, dr_1)$ is due to the field; it is is small.

We should note that the quotient $Q\colon = \sin\delta/\sin\omega$ requires a special care, because its derivative is not small: $dQ = \mathcal{O}(\varepsilon\, d\tau)$, as it follows from (3.11). However we note that in all the expressions (3.15)–(3.16) the fraction $\sin\delta/\sin\omega$ is multiplied either by $\sin\delta = \mathcal{O}(\varepsilon\tau)$ or by $dv = \mathcal{O}(\varepsilon\tau\, dr)$, thus dQ will be always suppressed by a small factor. Then the direct proof of curvature bounds (see the proof of equation (B.2) in [12]) can be carried over to our case; we leave the details to the reader. Thus, the corrections to the second order derivatives due to the external field $\mathbf{E}$ are all relatively small.

Next the proof of (B.2) in [12] uses the value $\mathcal{B}$, the curvature of the orthogonal cross-section of the wave front corresponding to the unstable curve right before the collision with $\partial\mathcal{D}$. We cannot use it here, so it has to be eliminated from the above proof as follows. First,

$$d^2\varphi_n/dr_n^2 = \cos\varphi_n d\mathcal{B}_n/dr_n + D_n$$

where $|D_n| \le D < \infty$ are bounded (see page 169 in [12]). Second it was proved on page 171 in [12] that

$$|d\mathcal{B}_n/dr_n| = \theta_n(w_n/w_{n-1})|d\mathcal{B}_{n-1}/dr_{n-1}| + R_n$$

where $|\theta_n| \le \theta < 1$, $|R_n| \le R < \infty$, and $0 < w_{\min} < w_n < w_{\max} < \infty$ are bounded away from zero and infinity. Combining the above formulas we see that

$$\left|\frac{d^2\varphi_n}{dr_n^2}\right| \le \theta\frac{\cos\varphi_n}{\cos\varphi_{n-1}}\frac{w_n}{w_{n-1}}\left[\left|\frac{d^2\varphi_{n-1}}{dr_{n-1}^2}\right| + D_{n-1}\right] + \theta\frac{w_n}{w_{n-1}}|R_n| + |D_n|.$$

The lemma now follows easily. □

Next, to ensure distortion control we need to construct homogeneity strips in $\mathcal{M}$, in a standard way:

$$\begin{aligned}
\mathbb{H}_j &= \{(r,\varphi)\colon \tfrac{\pi}{2} - j^{-2} < \varphi < \tfrac{\pi}{2} - (j+1)^{-2}\} \quad \forall j \ge j_0 \\
\mathbb{H}_0 &= \{(r,\varphi)\colon -\tfrac{\pi}{2} + j_0^{-2} < \varphi < \tfrac{\pi}{2} - j_0^{-2}\}, \\
\mathbb{H}_{-j} &= \{(r,\varphi)\colon -\tfrac{\pi}{2} + (j+1)^{-2} < \varphi < -\tfrac{\pi}{2} + j^{-2}\} \quad \forall j \ge j_0
\end{aligned} \tag{4.5}$$

where $j_0 > 1$ is a large constant, see [9, p. 216] and [17, Section 5.3]. We cut $\mathcal{M}$ along their boundaries, i.e. replace $\mathcal{M}$ with a countable union of the above strips. Accordingly, unstable curves must respect these new boundaries, i.e. each unstable curve must lie in one of the strips. If an unstable curve crosses several strips, it must be cut into pieces by the boundaries of the strips.

Lemma 4.2 (Distortion bounds). *There is a constant $C = C(\mathcal{D}) > 0$ such that for any unstable curve W and any point $X_1 = (\varphi_1, r_1) \in W_1$ on its image*

$$\left|\frac{d\ln \mathcal{J}_{W_1}\mathcal{F}_\varepsilon^{-1}(X_1)}{dr_1}\right| \le \frac{C}{|W_1|^{2/3}} \tag{4.6}$$

The first construction of homogeneity strips (4.5) and the first proof of distortion bounds were given in [7]. A more recent and direct proof is given in [12]; see equation (B.3) there. That proof can be adapted to our case because the corrections due to the field are small, as we explained above. □

We emphasize that all the constants in Lemmas 4.1 and 4.2 are uniform in ε.

Next we turn to *stable* vectors and stable curves. The estimate (3.20) is insufficient for the control over the contraction of stable vectors. To estimate contraction rates, we use the Jacobian of $D\mathcal{F}_\varepsilon$:

Lemma 4.3. *In terms of differential forms, we have*

$$v_1 \cos\varphi_1 \, dr_1 \wedge d\varphi_1 = v \cos\varphi \, dr \wedge d\varphi. \tag{4.7}$$

Proof. It follows from (3.15)–(3.16) that

$$\begin{aligned} v_1\tau \cos\varphi_1 \, dr_1 \wedge d\varphi_1 = v\tau \big[&\cos(\varphi-\delta)\cos\delta - \sin\delta\cos\delta\sin\varphi \\ &- \sin^2\delta \sin\varphi \cot\omega\big] dr \wedge d\varphi \\ &- \big(v\tau^2 \sin\delta \sin\omega_1/\sin\omega\big) dv \wedge d\varphi \end{aligned} \tag{4.8}$$

Observe that

$$\cos(\varphi-\delta)\cos\delta = \cos\varphi - \sin^2\delta\cos\varphi + \sin\delta\cos\delta\sin\varphi,$$

therefore (4.8) becomes

$$\begin{aligned} v_1\tau \cos\varphi_1 \, dr_1 \wedge d\varphi_1 = &\, v\tau\cos\varphi \, dr \wedge d\varphi \\ &- v\tau \sin^2\delta \big[\cos\varphi + \sin\varphi\cot\omega\big] dr \wedge d\varphi \\ &- \big(v\tau^2 \sin\delta\sin\omega_1/\sin\omega\big) dv \wedge d\varphi \end{aligned} \tag{4.9}$$

Lastly, we note that

$$\cos\varphi + \sin\varphi\cot\omega = \sin(\omega+\varphi)/\sin\omega = \cos\gamma/\sin\omega,$$

and use equation (3.17) and the second equation in (3.6). □

When $\varepsilon = 0$, then $v = v_1 = 1$ and $\delta = 0$, and (4.7) becomes

$$\cos\varphi_1 \, dr_1 \wedge d\varphi_1 = \cos\varphi \, dr \wedge d\varphi,$$

which shows that the billiard map $\mathcal{F}_0$ preserves the measure

$$d\nu_0 = \cos\varphi \, dr \, d\varphi \tag{4.10}$$

and is positively oriented in the $r\varphi$ coordinates (these are standard facts [17]). The map $\mathcal{F}_\varepsilon$, with respect to the measure (4.10) has (local) Jacobian

$$\nu_0(\mathcal{F}_\varepsilon(dX))/\nu_0(dX) = v/v_1 = 1 + \mathcal{O}(\varepsilon\tau). \tag{4.11}$$

One can also explain (4.11) as follows: the dynamics (2.2) is Hamiltonian and preserves Liouville measure (volume) in the 4-dimensional phase space $\tilde{\mathcal{D}} \times \mathbb{R}^2$. It obviously expands in the flow direction, between the two collisions, by a factor of v_1/v, thus it contracts areas in the orthogonal directions by a factor of v/v_1, and the measure ν_0 corresponds to the area in the directions orthogonal to the velocity vector.

Now we can analyze the contraction of stable vectors. The billiard map $\mathcal{F}_0$ is known to have a family of stable cones defined by

$$-\infty < C_1 \le d\varphi/dr \le C_2 < 0, \tag{4.12}$$

where $C_1 < C_2$ are some negative constants. Stable vectors $dX = (dr, d\varphi)$ are contracted by a factor

$$\|D\mathcal{F}_0(dX)\|_*/\|dX\|_* \le \big(1 + a/\cos\varphi\big)^{-1} < 1 \tag{4.13}$$

for some constant $a = a(\mathcal{D}) > 0$, where $\|dX\|_*$ is again the adapted metric (4.3).

Our estimate (3.20) implies that $\mathcal{F}_\varepsilon$, being close to $\mathcal{F}_0$, also contracts stable vectors defined by (4.12), and the contraction factor also satisfies (4.13), with a possibly smaller constant $a > 0$.

For the billiard map $\mathcal{F}_0$, the contraction factor of stable vectors satisfies a more accurate asymptotic formula

$$\frac{(dr_1^2 + d\varphi_1^2)^{1/2}}{(dr^2 + d\varphi^2)^{1/2}} \asymp \frac{dr_1}{dr} \asymp \frac{\cos\varphi}{\tau}, \tag{4.14}$$

see [17, Section 4.4]. The same is true for our map. Indeed, due to (4.11) the inverse maps $D\mathcal{F}_\varepsilon^{-1}$ and $D\mathcal{F}_0^{-1}$ are also close to each other, hence they expand images of stable vectors at nearly the same rates. These facts also follow from the 'local' time reversibility of our dynamics described next.

5. Local time reversibility, overlaps and gaps

It is helpful to note that the map $\mathcal{F}_\varepsilon$ is (locally) time reversible in the following sense.

Let $\mathcal{I}\colon \mathcal{M} \to \mathcal{M}$ denote the standard involution; it acts by

$$\mathcal{I}\colon (r, \varphi) \mapsto (r, -\varphi),$$

i.e. it takes $(\mathbf{q}, \mathbf{v}) \in \mathcal{M}$ to $(\mathbf{q}, \mathbf{v}') \in \mathcal{M}$, so that the vector $\mathbf{v}'$ is obtained by reflecting $\mathbf{v}$ across the normal line to $\partial\mathcal{D}$ at the point $\mathbf{q}$. Note that $\mathcal{I}^{-1} = \mathcal{I}$.

Now consider any point $(r, \varphi) \in \mathcal{M}$ that starts on a scatterer $B \subset \mathcal{D}$ and whose trajectory lands on another scatterer $B_1 \subset \mathbb{R}^2$, which is in another cell containing some domain $\mathcal{D}_i$ (Figure 5). Its initial velocity $\mathbf{v}$ and the final velocity $\mathbf{v}_1$ (right before landing) satisfy

$$\|\mathbf{v}\|^2 - 2\varepsilon x = \|\mathbf{v}_1\|^2 - 2\varepsilon x_1 = 1,$$

where $(x, y) \in \partial B$ denotes the starting point and $(x_1, y_1) \in \partial B_1$ the landing point. The domain $\mathcal{D}_i$ is obtained from $\mathcal{D}$ by translation along some vector $\mathbf{Z}_i = (Z_{i,x}, Z_{i,y})$. Our dynamics requires that we project the reflection point from ∂B_1 back onto $\mathcal{D}$ under $\tilde{\pi}$, i.e. the point (x_1, y_1) will be moved to (x_1', y_1') so that $x_1' = x_1 - Z_{i,x}$. Note also that

$$B_1' = \tilde{\pi}(B_1) = B_1 - \mathbf{Z}_i$$

is a scatterer in the central cell $\mathcal{K}$ and $(x_1', y_1') \in \partial B_1'$. If we translate the precollisional vector $\mathbf{v}_1$ from ∂B_1 to $\partial B_1'$ along the vector $-\mathbf{Z}_i$, its total energy becomes

$$\tfrac{1}{2}\,\|\mathbf{v}_1\|^2 - \varepsilon(x_1 - Z_{i,x}) = \tfrac{1}{2} + \varepsilon Z_{i,x}.$$

Let us now reverse the velocity vector $\mathbf{v}_1$ attached to $\partial B_1'$ and let it move under the field ε. Clearly its trajectory will be the translate, under the vector $-\mathbf{Z}_i$, of the previous trajectory (from (x, y) to (x_1, y_1)), but now it is traversed backwards. It will land at point $(x', y') = (x - Z_{i,x}, y - Z_{i,y})$ on a scatterer $B - \mathbf{Z}_i$ in a cell containing some domain $\mathcal{D}_j$; see Figure 5.

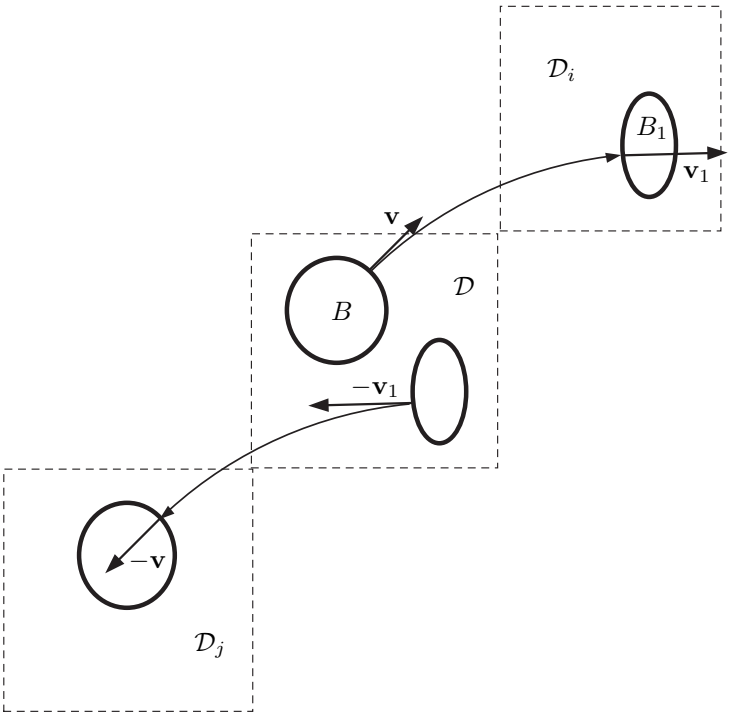

FIGURE 5. Weak time reversibility.

We emphasize that in the above analysis the new total energy

$$\mathcal{E} = \mathcal{E}_i = \tfrac{1}{2} + \varepsilon Z_{i,x} \tag{5.1}$$

will be the same for all points (r, φ) starting on a given scatterer, B, and landing on another given scatterer, B_1. This implies that

$$\mathcal{F}_{\mathcal{E},\varepsilon} \circ \mathcal{I} \circ \mathcal{F}_\varepsilon = \mathcal{I}, \tag{5.2}$$

where $\mathcal{F}_{\mathcal{E},\varepsilon}$ denotes the collision map similar to $\mathcal{F}_\varepsilon$, but constructed for the dynamics with the total energy $\mathcal{E}$, instead of $1/2$. Clearly our choice of $\mathcal{E} =$

1/2 for the total energy in (2.1) was quite arbitrary, and any other constant would give us a map with similar properties.

Equation (5.2) can be rewritten as

$$\mathcal{F}_\varepsilon^{-1} = \mathcal{I} \circ \mathcal{F}_{\mathcal{E},\varepsilon} \circ \mathcal{I} \tag{5.3}$$

which is only valid locally, on the set of points (r_1, φ_1) that start from the scatterer B and land on the scatterer B_1; the constant $\mathcal{E}$ is computed by (5.1) for the given pair of scatterers B and B_1.

Still, the local time reversibility in the above sense is helpful. In particular, it shows that since $\mathcal{F}_{\mathcal{E},\varepsilon}$ expands unstable vectors, $\mathcal{F}_\varepsilon$ will contract stable vectors (i.e. those that are the images of unstable vectors under $\mathcal{I}$).

Given a pair of scatterers B and B_1, the set of points (r_1, φ_1) that have come from B and land on B_1 is bounded by the images of points that make grazing (tangential) collisions either with B or with some other scatterers on their way from B to B_1. Grazing collisions are described by the lines $\varphi = \pm\pi/2$, hence their images are unstable curves. So this set of points is bounded by unstable curves and possibly by some segments of the lines $\varphi = \pm\pi/2$.

Similarly, the set of points (r, φ) that start from B and land on B_1 is bounded by stable curves (as well as some parts of the lines $\varphi = \pm\pi/2$); this follows from our local time reversibility.

Thus the space $\mathcal{M}$ is naturally partitioned into a finite collection of domains, $\mathcal{M} = \cup\mathcal{M}_i^+$, on each of which $\mathcal{F}_\varepsilon$ is smooth (for a moment, let us forget that $\mathcal{M}$ was divided into homogeneity strips (4.5)). The domains $\mathcal{M}_i^+$ are bounded by $\partial\mathcal{M} = \{\varphi = \pm\pi/2\}$ and by some smooth stable curves. The set $\mathcal{S}^+ = \cup\partial\mathcal{M}_i^+$ is the singularity set for the map $\mathcal{F}_\varepsilon$.

The images $\mathcal{M}_i^- = \mathcal{F}_\varepsilon(\mathcal{M}_i^+)$ are also domains in $\mathcal{M}$ on which $\mathcal{F}_\varepsilon^{-1}$ is (locally) defined and smooth. The domains $\mathcal{M}_i^-$ are bounded by $\partial\mathcal{M} = \{\varphi = \pm\pi/2\}$ and by some smooth unstable curves.

The billiard map $\mathcal{F}_0$ has all these properties, too, but its domains $\mathcal{M}_i^-$ make a partition of $\mathcal{M}$, i.e. they are disjoint and cover the entire $\mathcal{M}$. Their boundaries are singularities for the inverse map $\mathcal{F}_0^{-1}$.

But for our map $\mathcal{F}_\varepsilon$, the domains $\mathcal{M}_i^-$ may overlap and they may not cover the entire $\mathcal{M}$, i.e. some gaps are left in between.

Fig. 6 shows how overlaps occur. In that figure (unlike Fig. 5), we draw trajectories as if they started from different domains $\mathcal{D}_i, \mathcal{D}_j$ but landed on the same scatterer in the main domain $\mathcal{D}$. Two trajectories shown land at a point $\mathbf{q} \in \partial B \subset \mathcal{K}$. One (the solid line) starts from a scatterer B_1 (in $\mathcal{D}_i$), and the other (the dashed line) – from another scatterer B_2 (in $\mathcal{D}_j$) and it comes infinitesimally close to B_1.

Since $Z_{i,x} < Z_{j,x}$, the first trajectory is less energetic (thus more curved) than the segment of the second trajectory running between B_1 and B. Though both trajectories land at the same point $\mathbf{q}$, they arrive at different incidence angles φ_1 and φ_2, and the difference $|\varphi_1 - \varphi_2|$ corresponds to the size of overlap of the respective domains $\mathcal{M}_{i_1}^-$ and $\mathcal{M}_{i_2}^-$ (one consists of trajectories

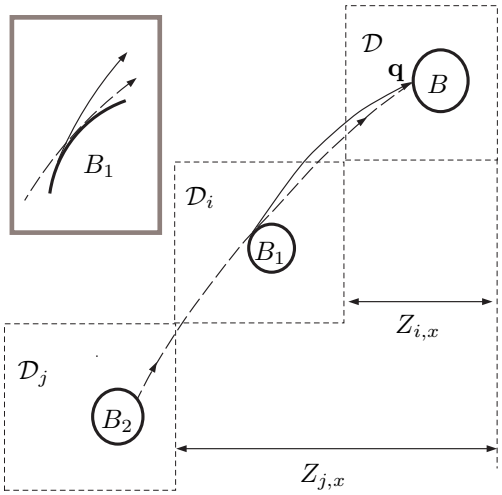

FIGURE 6. How the images can overlap. Both the solid and dashed trajectories are tangent to the scatterer B_1 (see the inset).

coming to ∂B from ∂B_1, and the other – from ∂B_2). An elementary analysis shows that the size of the overlap (in the φ direction on $\mathcal{M}$) is

$$\Delta\varphi = \mathcal{O}\big(\varepsilon^2 |Z_{ij,x}|(|Z_{i,y}| + 1)\big), \tag{5.4}$$

where $Z_{ij,x} = Z_{i,x} - Z_{j,x}$ is the displacement in the x direction between the domains $\mathcal{D}_i$ and $\mathcal{D}_j$, and $Z_{i,y}$ is the displacement in the y direction between the domains $\mathcal{D}_i$ and $\mathcal{D}$. So for finite horizon Lorentz gases we simply have $\Delta\varphi = \mathcal{O}(\varepsilon^2)$. In the infinite horizon case (5.4) leads to larger overlaps, to be described later.

Similarly, Fig. 7 shows how gaps occur. The trajectory coming from B_1 is less energetic (i.e., more curved) than the one coming from B_2. The difference between their angles of incidence at the landing point $\mathbf{q}$ corresponds to the size of the gap between the respective domains $\mathcal{M}^-_{i_1}$ and $\mathcal{M}^-_{i_2}$. Again an elementary analysis shows that the size of the gap is given by the same formula (5.4), so for finite horizon Lorentz gases the gaps are $\mathcal{O}(\varepsilon^2)$. In the infinite horizon case, gaps may be larger, see below.

Remark. As we mentioned in Section 2, the fundamental domain $\mathcal{K}$ can be doubled, tripled, etc. We describe how "multiplying" $\mathcal{K}$ would affect the gaps and overlaps. First, they occur only when trajectories cross from one copy of $\mathcal{K}$ to another. So if we make $\mathcal{K}$ larger, we would have fewer gaps and overlaps. But since $Z_{ij,x}$ in (5.4) corresponds to the size of $\mathcal{K}$ (in the x direction), our gaps and overlaps would get wider. Roughly speaking, if we double the size of $\mathcal{K}$, then the space $\mathcal{M}$ also doubles in size, and in the new, bigger $\mathcal{M}$ half of the gaps would close up and disappear, half of the overlaps would disappear,

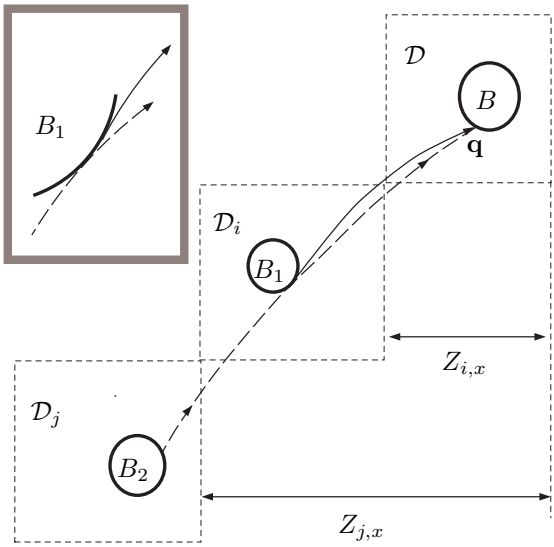

FIGURE 7. Creation of a gap between the images. Both the solid and dashed trajectories are tangent to the scatterer B_1 (see the inset).

too, but the other half of the gaps and overlaps would get about twice as wide. It seems that such a change would not alter the basic properties of our dynamics, though.

6. Structure of singularities

Next we analyze the singularities of the map $\mathcal{F}_\varepsilon$. We begin by recalling the properties of the singularities of the billiard map $\mathcal{F}_0$.

When the horizon is finite, the singularity set $\mathcal{S}$ of $\mathcal{F}_0$ is a finite union of smooth compact stable curves. They have a *continuation property* ([17, Section 4.9]), i.e. each curve $S \subset \mathcal{S}$ either terminates on the boundary of $\mathcal{M}$ (i.e., on the lines $\varphi = \pm\pi/2$), or it is a part of a longer monotonic continuous curve $S' \subset \mathcal{S}$ that extends (continues) to the boundary of $\mathcal{M}$ (of course, then S' is a union of several smooth components of $\mathcal{S}$). In other words, $\mathcal{S}$ divides $\mathcal{M}$ into domains $\mathcal{M}_i^+$ with piecewise smooth boundaries ('curvilinear polygons') such that at their corner points the interior angles are $\leq \pi$ (polygons are 'convex').

The singularity set for our map $\mathcal{F}_\varepsilon$ with finite horizon has all the same properties. This follows from the local time reversibility.

For the billiard map $\mathcal{F}_0$, the images $\mathcal{M}_i^- = \mathcal{F}_\varepsilon(\mathcal{M}_i^+)$ are also 'convex' curvilinear polygons bounded by smooth compact *unstable* curves. The same remains true for the map $\mathcal{F}_\varepsilon$, except the domains $\mathcal{M}_i^-$ no longer make a

partition of $\mathcal{M}$: some of them overlap by $\mathcal{O}(\varepsilon^2)$ near their boundaries, and between others there are gaps of size $\mathcal{O}(\varepsilon^2)$.

In the infinite horizon case, the singularity set $\mathcal{S}$ of the billiard map $\mathcal{F}_0$ is a *countable* union of smooth compact stable curves, which accumulate near finitely many points $X \in \mathcal{M}$ whose trajectories run along the borders of the infinite corridors ([17, Section 4.10]). These are exactly the points entering the formula (1.5); see one of them in Figure 8. The singularity curves near the fixed points X form a cell structure [17] whose features essentially determine global properties of the map $\mathcal{F}_0$.

Unlike $\mathcal{F}_0$, our map $\mathcal{F}_\varepsilon$ has finitely many singularity lines even in the infinite horizon case, because the length of the free path is always bounded (Lemma 2.1). But the number of singularity lines is $\mathcal{O}(\varepsilon^{-1/2})$, i.e. it is not uniformly bounded. The structure of the singularity lines and the corresponding cells is similar to that of the collision map for the thermostatted dynamics [15]. We briefly describe it next.

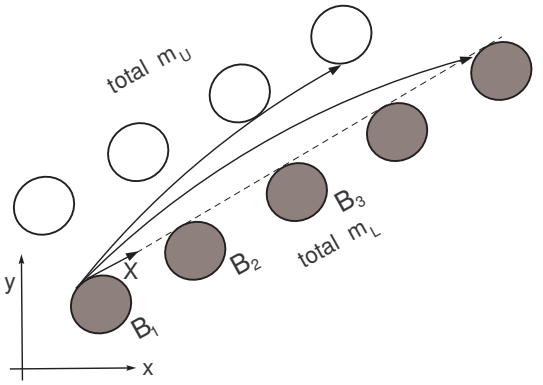

FIGURE 8. A row of scatterers forming the border of an infinite corridor.

Trajectories leaving $\mathcal{D}$ into an infinite corridor can land on scatterers on either side of the corridor; see Fig. 8. The number of scatterers that our trajectories can reach is $\mathcal{O}(\varepsilon^{-1/2})$, due to Lemma 2.1. More precisely, let m_U denote the number of reachable scatterers on the upper side of the corridor, and let m_L denote those on the lower side; see Fig. 8. Since our trajectories are parabolas, an elementary computation shows that

$$m_U \sim C_1/\sqrt{\varepsilon}, \qquad m_L \sim C_2/\sqrt{\varepsilon}, \qquad 0 < C_1 < C_2$$

The singularity lines near the point marked by X in Fig. 8 are shown in Fig. 9. The long singularity curve S corresponds to grazing collisions with the very next scatterer in the corridor (marked by B_2 in Fig. 8). The short singularity curves are made by grazing collisions with other scatterers in the corridor.

The regions between singularity curves (cells) are made by trajectories landing on a particular scatterer. Thus, the cells can be naturally numbered by $1, \dots, m_U$ (corresponding to the upper scatterers) and $1, \dots, m_L$ (for the lower scatterers). Accordingly, we denote the cells by $D_1^{(U)}, \dots, D_{m_U}^{(U)}$ and $D_1^{(L)}, \dots, D_{m_L}^{(L)}$ (here U and L stand for 'Upper' and 'Lower', respectively).

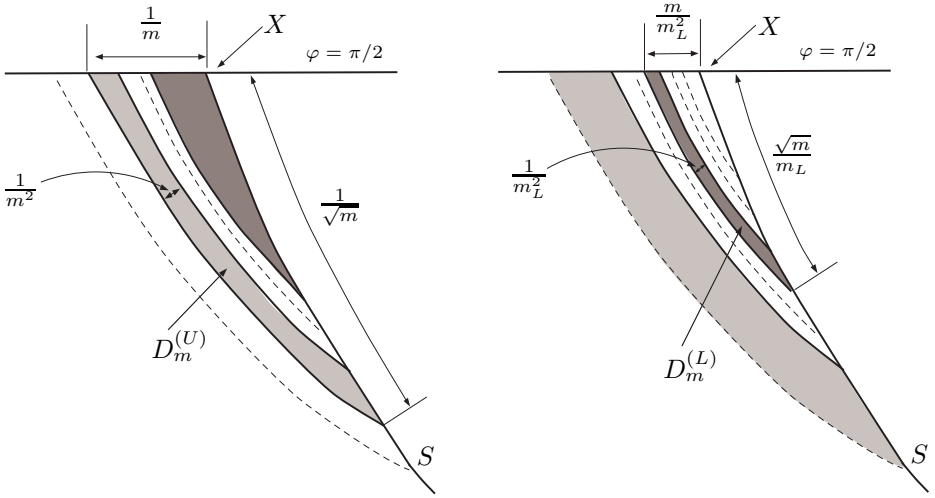

FIGURE 9. Singularity curves and cells. On the left, an 'upper' cell $D_m^{(U)}$ is shown, with all its dimensions, in light grey; the union of all the 'lower' cells $D_m^{(L)}$'s is painted dark grey. On the right, a 'lower' cell $D_m^{(L)}$ is shown, with all its dimensions, in dark grey; the union of all the 'upper' cells $D_m^{(U)}$'s is painted light grey.

In Fig. 9 the cells are depicted as follows. First (farther from S) come the cells $D_1^{(U)}, \dots, D_{m_U}^{(U)}$ (in this order). The height of $D_m^{(U)}$ is $\asymp 1/\sqrt{m}$ and its width is $\asymp 1/m^2$, just like in classical billiards with infinite horizon, see e.g. [17, Section 4.10]. Unstable curves inside $D_m^{(U)}$ are expanded by a factor $\Lambda_m^{(U)} \geq cm^{3/2}$ for some $c > 0$, due to (4.4), in which $\tau \asymp m$ and $\cos\varphi_1 = \mathcal{O}(m^{-1/2})$.

Second (closer to S) come the cells $D_{m_L}^{(L)}, \dots, D_1^{(L)}$ (in the reverse order; the cell $D_1^{(L)}$ is adjacent to the point X). The height of $D_m^{(L)}$ is $\asymp \sqrt{m}/m_L$ and its width is $\asymp 1/m_L^2$. Unstable curves inside $D_m^{(L)}$ are expanded by a factor $\Lambda_m^{(L)} \geq cm_L\sqrt{m}$ for some $c > 0$, again due to (4.4), in which $\tau \asymp m$ and $\cos\varphi_1 = \mathcal{O}(\sqrt{m}/m_L)$.

We record the following formulas for the measures of the cells:

$$\nu_0\big(D_m^{(U)}\big) \asymp 1/m^3, \qquad \nu_0\big(D_m^{(L)}\big) \asymp m/m_L^4 \asymp m\varepsilon^2 \tag{6.1}$$

Indeed, the billiard measure ν_0 is smooth and has density $\cos\varphi$, thus the measure of each cell is of the same order of magnitude as the product width$\times$(height)^2.

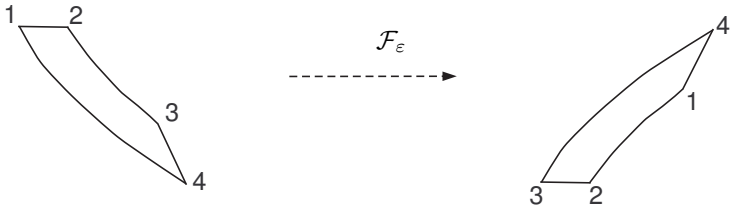

FIGURE 10. The map $\mathcal{F}_0$ transforms a cell D_m into a similar-looking domain. The corners of D_m and their respective images are numbered to indicate the action of $\mathcal{F}_0$.

For the billiard map $\mathcal{F}_0$, there are no 'lower' cells, but there are infinitely many 'upper' cells $D_m^{(U)} = D_m$, $m = 1, 2, \ldots$, each having the shape and size as described above. The map $\mathcal{F}_0$ transforms cells into similar-looking domains, but the images are bounded by unstable curves; see Fig. 10 and more details in [17, Section 4.10]. The image $\mathcal{F}_0(D_m)$ has the same dimensions as D_m, so the expansion factor of the map $\mathcal{F}_0$ acting on unstable curves in D_m is

$$\Lambda \sim \frac{\text{height of } \mathcal{F}_0(D_m)}{\text{width of } D_m} \sim \frac{\text{height of } D_m}{\text{width of } D_m} \asymp m^{3/2} \tag{6.2}$$

This rule can be used to verify our previous formulas for the expansion factor of the map $\mathcal{F}_\varepsilon$ in $D_m^{(U)}$ and $D_m^{(L)}$.

For our map, the domains $\mathcal{F}_\varepsilon(D_m^{(U)})$ and $\mathcal{F}_\varepsilon(D_m^{(L)})$ also look like the cells $D_m^{(U)}$ and $D_m^{(L)}$, respectively, and the images are also bounded by unstable curves. But, unlike $\mathcal{F}_0$, the images of cells under $\mathcal{F}_\varepsilon$ can overlap and there may be gaps between them.

Fig. 11 shows the images of cells depicted in Fig. 9. There are gaps of size $\asymp m\varepsilon^2$ between the images of neighboring upper cells $D_m^{(U)}$ and $D_{m+1}^{(U)}$. The image of each lower cell $D_m^{(L)}$ overlaps by $\asymp m\varepsilon^2$ with the images of the two neighboring lower cells. (Since $m\varepsilon^2$ is much less than the width of the m-th cell, only neighboring cells can overlap.) The image of each cell D_m (upper or lower) overlaps by $\asymp m\varepsilon^2$ with the region beyond (i.e., to the left of) the long singularity curve S^-. And there is a wide gap of size $\asymp \varepsilon$ between the image of the last upper cell $D_{m_U}^{(U)}$ and that of the last lower cell $D_{m_L}^{(L)}$. All these formulas follow from (5.4), which describes the extent of overlaps and gaps.

In some other cases, the images $\mathcal{F}_\varepsilon(D_m^{(U)})$ and $\mathcal{F}_\varepsilon(D_m^{(L)})$ may form a different structure: images of the upper cells may overlap (instead of leaving gaps in between), and images of the lower cells may leave gaps (instead of overlapping); it is also possible that the lower cells (and their images) are

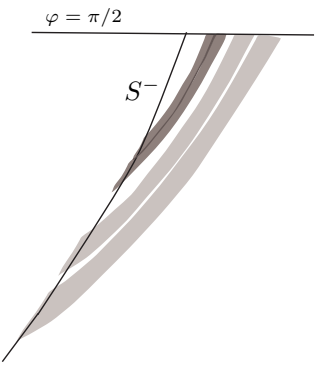

FIGURE 11. Images of cells under $\mathcal{F}_\varepsilon$. There is a narrow (white) gap between two (light grey) 'upper' cells. Two (dark grey) lower cells overlap along a black narrow strip between them. There is a wider white gap between the last (top) upper cell and the last (bottom) lower cell. All the cells overlap with the long curve S^- and stretch slightly beyond (to the left of) it.

missing altogether. But in all cases the sizes of gaps and overlaps are given by the same formula $\asymp m\varepsilon^2$ as above.

The total ν_0-measure of all the gaps and overlaps is

$$\nu_0(\text{gaps + overlaps}) \asymp \varepsilon\left[\frac{1}{\sqrt{m_U}}\right]^2 + \sum_{m=1}^{m_U} \frac{m\varepsilon^2}{(\sqrt{m})^2} + \sum_{m=1}^{m_L} m\varepsilon^2\left[\frac{\sqrt{m}}{m_L}\right]^2$$
$$\asymp \varepsilon^{3/2} + \varepsilon^{3/2} + \varepsilon^{3/2} \asymp \varepsilon^{3/2}, \tag{6.3}$$

where the first term accounts for the 'big' gap of width ε between the images of the last upper cell and the last lower cell (that gap has the largest measure of all our gaps and overlaps). We note that the height of every cell in (6.3) is squared to account for the density of ν_0, which is $\cos\varphi$.

7. Growth lemmas and standard families

Next we derive a key fact about the growth of unstable curves, known as Growth Lemma. Given an unstable curve W, let us denote by $W_i \subset W$ the connected components of $W \setminus \mathcal{S}$, i.e. the segments of W on which $\mathcal{F}_\varepsilon$ is smooth, and by Λ_i the (minimal) factor of expansion of W_i under $\mathcal{F}_\varepsilon$ in the adapted metric (4.3).

Lemma 7.1 (One-step expansion). *We have*

$$\liminf_{\delta_0 \to 0} \sup_{W:\ |W|<\delta_0} \sum_i \Lambda_i^{-1} < 1, \tag{7.1}$$

where the supremum is taken over unstable curves W of length $< \delta_0$.

The bound (7.1) is called the one-step expansion estimate [20, Section 5], it shows how much unstable curves stretch under *one* iteration of the map.

Proof. For dispersing billiards with finite horizon, the proof of (7.1) is standard (see [17, Lemma 5.56]), and it readily carries over to our dynamics with an external field. Without finite horizon, infinite corridors add new complications – it is possible that a short unstable curve W intersects many cells described above. Suppose W intersects cells $D_p^{(U)}$, $p_0 \le p \le m_U$, and $D_q^{(L)}$, $q_0 \le q \le m_L$, then

$$\sum_i \Lambda_i^{-1} \le \sum_{p=p_0}^{m_U} \frac{C}{p^{3/2}} + \sum_{q=q_0}^{m_L} \frac{C}{m_L q^{1/2}} \le \frac{C}{p_0^{1/2}} + \frac{C}{m_L^{1/2}}.$$

If W is small, then p_0 must be large, and the above bound is $\ll 1$. This completes the proof of (7.1) in the infinite horizon case.

For simplicity, we have ignored additional singularities that come from the artificially constructed boundaries of the homogeneity strips (4.5). Taking them into account would make the analysis somewhat more complicated, but the final result would remain the same as for billiards; see [8, Section 8] and [20, Section 7]. □

The one-step expansion estimate (7.1) implies several properties known collectively as Growth Lemmas, see [17, Chapter 5], [20, Section 4.7], [9, Proposition 5.3], [12, Lemma 4.10], and the proofs therein. We state their most common versions below.

Given an unstable curve W, we denote by m_W the Lebesgue measure on it. For every $n \ge 0$, its image $\mathcal{F}_\varepsilon^n(W)$ is a finite or countable union of unstable curves (components), and for every $X \in W$ we denote by $W_n(X)$ the component containing the point $\mathcal{F}_\varepsilon^n(X)$. Now let

$$r_n(X) = \operatorname{dist}\big(\mathcal{F}_\varepsilon^n(X), \partial W_n(X)\big) \tag{7.2}$$

denote the distance from the point $\mathcal{F}_\varepsilon^n(X)$ to the nearer endpoint of $W_n(X)$. Clearly, r_n is a function on W that characterizes the size of the components of $\mathcal{F}_\varepsilon^n(W)$. We also denote by $\Lambda > 1$ the hyperbolicity constant, i.e. the minimal expansion factor of unstable curves in the adapted metric.

Lemma 7.2 ("Growth lemma"). *Unstable curves $W \subset \mathcal{M}$ have the following properties:*
(a) *There are constants $\vartheta_0 \in (0,1)$ and $c_1, c_2 > 0$, such that for all $n \ge 0$ and $\zeta > 0$*

$$m_W(r_n(X) < \zeta) \le c_1(\vartheta_0\Lambda)^n\, m_W(r_0 < \zeta/\Lambda^n) + c_2\zeta\, m_W(W)$$

(b) *There are constants $c_3, c_4 > 0$, such that if $n \ge c_3\big|\ln m_W(W)\big|$, then for any $\zeta > 0$ we have $m_W(r_n(X) < \zeta) \le c_4\zeta\, m_W(W)$.*

(c) *There are constants* $\vartheta_1 \in (0,1)$ $c_5, c_6 > 0$, *a small* $\zeta_0 > 0$ *such that for any* $n_2 > n_1 > c_5 \big|\ln m_W(W)\big|$ *we have*

$$m_W\Big(\max_{n_1<n<n_2} r_n(X) < \zeta_0\Big) \le c_6 \vartheta_1^{n_2-n_1} m_W(W).$$

For the proof and implications of this lemma we refer to [17, 20]. We emphasize that the lim inf in (7.1) and all the constants in Growth Lemma are independent of ε, i.e. the respective properties hold uniformly in ε.

In plain words, the Growth Lemma means that the images of any unstable curve W grow, on average, exponentially fast, until they reach a certain minimal average size, and then that minimal average size is maintained forever. More precisely, the proportion of small components (of size $< \zeta$) among all the components of $\mathcal{F}_\varepsilon^n(W)$ remains $\mathcal{O}(\zeta)$.

Such a fast expansion of unstable curves allows us to construct stable manifolds for the map $\mathcal{F}_\varepsilon$. A stable manifold W^s is a stable curve such that $\mathcal{F}_\varepsilon^n(W^s)$ is also a stable curve for every $n \ge 1$. In that case the size of $\mathcal{F}_\varepsilon^n(W^s)$ is $\le C\lambda^n$, where $\lambda < 1$ is the weakest contraction factor of stable curves.

Lemma 7.3. *Let* W *be an unstable curve and* m_W *the Lebesgue measure on it. For* m_W*-almost every point* $X \in W$ *there is a stable manifold* $W^s(X)$ *passing through* X*. Moreover, for any* $\zeta > 0$

$$m_W\big(X \in W\colon r^s(X) < \zeta\big) \le C\zeta,$$

where

$$r^s(X) = \operatorname{dist}\big(X, \partial W^s(X)\big)$$

denotes the distance from X *to the nearer endpoint of the curve* $W^s(X)$*, and* $C > 0$ *a constant.*

Proof. It is standard (see, e.g., [17, Section 4.12]) that

$$r^s(X) \ge c \min_{n\ge 0} \Lambda^n \operatorname{dist}(\mathcal{F}_\varepsilon^n(X), \partial\mathcal{M})$$

for some constant $c > 0$, and we obviously have

$$\operatorname{dist}(\mathcal{F}_\varepsilon^n(X), \partial\mathcal{M}) \ge c' r_n(X)$$

for some constant $c' > 0$. Thus if $r^s(X) < \zeta$, then $r_n(X) < c''\zeta\Lambda^{-n}$ for some $n \ge 0$, where $c'' > 0$ is another constant. Due to Growth Lemma (a) such points make a set of m_W-measure $\mathcal{O}(\varepsilon)$. □

As usual, stable manifolds $W^s \subset \mathcal{M}$ cannot cross each other, and the foliation of $\mathcal{M}$ into stable manifolds is a measurable partition; see [17, Section 5.1]. That foliation is absolutely continuous in the following sense.

Let W_1 and W_2 be two nearby unstable curves and W^s a stable manifold crossing each W_i in a point X_i, then the Jacobian of the holonomy map $\mathbf{h}\colon W_1 \to W_2$ at X_1 satisfies

$$e^{-C(\gamma+[\operatorname{dist}(X_1,X_2)]^{1/3})} \le \mathcal{J}\mathbf{h}(X_1) \le e^{-C(\gamma+[\operatorname{dist}(X_1,X_2)]^{1/3})} \tag{7.3}$$

where γ is the angle between the tangent vectors to W_1 and W_2 at the points X_1 and X_2, respectively. The property (7.3) is proved for the billiard map

$\mathcal{F}_0$ in [17, Theorem 5.42], and it extends to our case because the corrections to derivatives due to the field are $\mathcal{O}(\tau\varepsilon)$, as we established in the proof of Lemma 4.1.

Next, for any two points $X, Y \in \mathcal{M}$ we denote by $\mathbf{s}_+(X,Y) \geq 0$ the future separation time: it is the first time when the images $\mathcal{F}_\varepsilon^n(X)$ and $\mathcal{F}_\varepsilon^n(Y)$ land on different scatterers or in different homogeneity strips (i.e. the first time when $\mathcal{F}_\varepsilon^{n-1}(X)$ and $\mathcal{F}_\varepsilon^{n-1}(Y)$ belong to different connected components of $\mathcal{M} \setminus \mathcal{S}$). Observe that if X and Y lie on one unstable curve $W \subset \mathcal{M}$, then $\operatorname{dist}(X,Y) \leq C\Lambda^{-\mathbf{s}_+(X,Y)}$, cf. [17, Eq. (5.32)]. Now (7.3) implies (just like in the case billiards; see Section 5.8, in particular Proposition 5.48 of [17]) that for any pair of nearby unstable curves W_1, W_2 and any $X, Y \in W_1$

$$|\ln \mathcal{J}\mathbf{h}(X) - \ln \mathcal{J}\mathbf{h}(Y)| \leq C\vartheta^{\mathbf{s}_+(X,Y)}, \tag{7.4}$$

for some constant $\vartheta < 1$ (in fact, $\vartheta = \Lambda^{-1/6}$). Following Young [31, p. 597], we call the property (7.4) the 'dynamically defined Hölder continuity' of $\mathcal{J}\mathbf{h}$.

Next we define a class of probability measures supported on unstable curves. A *standard pair* $\ell = (W, \rho)$ is an unstable curve $W \subset \mathcal{M}$ with a probability measure $\mathbb{P}_\ell$ on it, whose density ρ (with respect to the Lebesgue measure on W) satisfies

$$|\ln \rho(X) - \ln \rho(Y)| \leq C_{\mathrm{r}}\, \Lambda^{-\mathbf{s}_+(X,Y)}. \tag{7.5}$$

Here $C_{\mathrm{r}} > 0$ is a sufficiently large constant (independent of ε). For any standard pair $\ell = (W, \rho)$ and $n \geq 1$ the image $\mathcal{F}_\varepsilon^n(W)$ is a finite or countable union of components on which the density of the measure $\mathcal{F}_\varepsilon^n(\mathbb{P}_\ell)$ satisfies (7.5), due to the distortion bounds (Lemma 4.2); see a proof in [17, Proposition 7.12]. Hence the image of a standard pair under $\mathcal{F}_\varepsilon^n$ is a countable family of standard pairs (with a factor measure).

More generally, a *standard family* is an arbitrary (countable or uncountable) collection $\mathcal{G} = \{\ell_\alpha\} = \{(W_\alpha, \rho_\alpha)\}$, $\alpha \in \mathfrak{A}$, of standard pairs with a probability factor measure $\lambda_\mathcal{G}$ on the index set $\mathfrak{A}$. Such a family induces a probability measure $\mathbb{P}_\mathcal{G}$ on the union $\cup_\alpha W_\alpha$ (and thus on $\mathcal{M}$) defined by

$$\mathbb{P}_\mathcal{G}(B) = \int \mathbb{P}_\alpha(B \cap W_\alpha)\, d\lambda_\mathcal{G}(\alpha) \qquad \forall B \subset \mathcal{M}.$$

Any standard family $\mathcal{G}$ is mapped by $\mathcal{F}_\varepsilon^n$ into another standard family $\mathcal{G}_n = \mathcal{F}_\varepsilon^n(\mathcal{G})$, and $\mathbb{P}_{\mathcal{G}_n} = \mathcal{F}_\varepsilon^n(\mathbb{P}_\mathcal{G})$.

For every $\alpha \in \mathfrak{A}$, any point $X \in W_\alpha$ divides the curve W_α into two pieces, and we denote by $r_\mathcal{G}(X)$ the length of the shorter one. Now the quantity

$$\mathcal{Z}_\mathcal{G} = \sup_{\zeta > 0} \zeta^{-1} \mathbb{P}_\mathcal{G}(r_\mathcal{G} < \zeta)$$

reflects the 'average' size of curves W_α in $\mathcal{G}$, and we have

$$\mathcal{Z}_\mathcal{G} \leq C \int \frac{d\lambda_\mathcal{G}(\alpha)}{|W_\alpha|} \tag{7.6}$$

see [17, Exercise 7.15]. We only consider standard families with $\mathcal{Z}_{\mathcal{G}} < \infty$. The growth lemma implies that for all $n \geq 0$ and some constant $\theta \in (0,1)$

$$\mathcal{Z}_{\mathcal{G}_n} \leq C(\theta^n \mathcal{Z}_{\mathcal{G}} + 1), \tag{7.7}$$

see a proof in [17, Proposition 7.17]; this estimate effectively asserts that standard families grow under $\mathcal{F}_\varepsilon^n$ exponentially fast.

We say that a standard pair (W, ρ) is *proper* if $|W| \geq \delta_{\mathrm{p}}$, where $\delta_{\mathrm{p}} > 0$ is a small but fixed constant. We say that a standard family $\mathcal{G}$ is *proper* if $\mathcal{Z}_{\mathcal{G}} \leq C_{\mathrm{p}}$, where C_{p} is a large but fixed constant (chosen so that a family consisting of a single proper standard pair is proper). We note that the image of a proper standard family under $\mathcal{F}_\varepsilon^n$ is proper for every $n \geq \text{const}=\text{const}(C, \theta)$.

We note that the measure ν_0 can be represented by a proper standard family. Indeed, foliating $\mathcal{M}$ by unstable curves and conditioning the measure ν_0 on them gives a standard family $\mathcal{G}_0$ such that $\mathbb{P}_{\mathcal{G}_0} = \nu_0$.

In systems with infinite horizon, trajectories starting in cells $D_m^{(U)}$ and $D_m^{(L)}$ have a long free flight – they travel the distance $\asymp m$ before landing on another scatterer. It is important to estimate the integral effect of the long free flights. Let A be the 'cell number' function on $\mathcal{M}$, i.e. $A = m$ on every cell $D_m^{(U)}$ and $D_m^{(L)}$ (and $A = 0$ on the rest of $\mathcal{M}$). It easily follows from (6.1) that

$$\nu_0(A) \asymp \sum_{m=1}^{m_U} \frac{m}{m^3} + \sum_{m=1}^{m_L} m^2 \varepsilon^2 = \mathcal{O}(1) \tag{7.8}$$

i.e. $\nu_0(A)$ is bounded uniformly in ε. Similarly,

$$\nu_0(A^2) \asymp \sum_{m=1}^{m_U} \frac{m^2}{m^3} + \sum_{m=1}^{m_L} m^3 \varepsilon^2 = \mathcal{O}(|\ln \varepsilon|), \tag{7.9}$$

and for any $k \geq 3$

$$\nu_0(A^k) \asymp \sum_{m=1}^{m_U} \frac{m^k}{m^3} + \sum_{m=1}^{m_L} m^{k+1} \varepsilon^2 = \mathcal{O}(\varepsilon^{-\frac{k-2}{2}}). \tag{7.10}$$

Let $\mathcal{G}$ be a proper standard family. Since $D_m^{(U)}$ has width $\asymp 1/m^2$, in the unstable direction, we have $\mathbb{P}_{\mathcal{G}}(D_m^{(U)}) = \mathcal{O}(1/m^2)$. Similarly, $\mathbb{P}_{\mathcal{G}}(D_m^{(L)}) = \mathcal{O}(1/m_L^2)$. Therefore

$$\mathbb{P}_{\mathcal{G}}(A) \leq \sum_{m=1}^{m_U} \frac{m}{m^2} + \sum_{m=1}^{m_L} \frac{m}{m_L^2} = \mathcal{O}(|\ln \varepsilon|), \tag{7.11}$$

and similarly

$$\mathbb{P}_{\mathcal{G}}(A^k) = \mathcal{O}(\varepsilon^{-\frac{k-1}{2}}), \tag{7.12}$$

which is not much worse than (7.8)–(7.10).

Next we estimate possible effect of gaps and overlaps on our integral formulas. Let $\nu_\diamond$ denote the measure ν_0 restricted to all gaps and overlaps between domains $\mathcal{M}_i^-$. Due to (6.3), its norm is $\|\nu_\diamond\| = \mathcal{O}(\varepsilon^{3/2})$. Gaps and overlaps are strips stretching in the unstable direction. We can foliate them by unstable curves, condition $\nu_\diamond$ on those curves, and get a 'standard family'

$\mathcal{G}_\diamond$ (though the norm of the corresponding measure $\mathbb{P}_{\mathcal{G}_\diamond}$ will be $\|\nu_\diamond\|$, rather than one). We can see directly that

$$\begin{aligned}\mathcal{Z}_{\mathcal{G}_\diamond} &= \sup_{\zeta>0} \zeta^{-1}\mathbb{P}_{\mathcal{G}_\diamond}(r_{\mathcal{G}_\diamond} < \zeta)\\ &\asymp \varepsilon^{1/4}\varepsilon + \sum_{m=1}^{m_U} m^{-1/2} m\varepsilon^2 + \sum_{m=1}^{m_L} \sqrt{m\varepsilon}\, m\varepsilon^2\\ &\asymp \varepsilon^{5/4}\end{aligned}$$

(in the middle line, the first term accounts for the gap of width ε between the last upper cell and the last lower cell, the first sum – for gaps/overlaps of width $m\varepsilon^2$ between the upper cells, and the second – the same for the lower cells; the factors $\varepsilon^{1/4}$, $m^{-1/2}$, and $\sqrt{m\varepsilon}$ simply account for the density $\cos\varphi$ of ν_0). Thus (7.11) now takes form

$$\mathbb{P}_{\mathcal{G}_\diamond}(A) = \mathcal{O}(\varepsilon^{5/4}|\ln\varepsilon|) \tag{7.13}$$

and (7.12) takes form

$$\mathbb{P}_{\mathcal{G}_\diamond}(A^k) = \mathcal{O}(\varepsilon^{\frac{5}{4}-\frac{k-1}{2}}) = \mathcal{O}(\varepsilon^{\frac{7-2k}{4}}). \tag{7.14}$$

Furthermore, the image $\mathcal{F}_\varepsilon^n(\mathcal{G}_\diamond)$ is a 'standard family' (with the same norm of the total measure, though) whose $\mathcal{Z}$-value can only decrease with n, due to (7.7), hence we have

$$\mathbb{P}_{\mathcal{G}_\diamond}(A \circ \mathcal{F}_\varepsilon^n) = \mathcal{O}(\varepsilon^{5/4}|\ln\varepsilon|). \tag{7.15}$$

for all $n \geq 1$. In the same way we can estimate the measure of gaps and overlaps in each cell $D_m^{(U)}$ or $D_m^{(L)}$. Since the width of the cell is $1/m^2$ or $1/m_L^2$, respectively, we have for all $n \geq 0$

$$\big(\mathcal{F}_\varepsilon^n \nu_\diamond\big)(D_m^{(U)}) = \mathcal{O}(\varepsilon^{5/4}/m^2) \tag{7.16}$$

and

$$\big(\mathcal{F}_\varepsilon^n \nu_\diamond\big)(D_m^{(U)}) = \mathcal{O}(\varepsilon^{5/4}/m_L^2) \tag{7.17}$$

Lastly, let $M_\diamond^-$ denote the union of the preimages of all the overlaps; this is the subset of $\mathcal{M}$ on which $\mathcal{F}_\varepsilon$ fails to be injective. We have seen in (6.3) that $\nu_0(D_m^{(U)} \cap M_\diamond^-) = \mathcal{O}(\varepsilon^2)$ and $\nu_0(D_m^{(L)} \cap M_\diamond^-) = \mathcal{O}(\varepsilon^2 m^2/m_L^2)$, hence

$$\int_{M_\diamond^-} A\, d\nu_0 \asymp \sum_{m=1}^{m_U} m\varepsilon^2 + \sum_{m=1}^{m_L} \varepsilon^2 m^3/m_L^2 = \mathcal{O}(\varepsilon). \tag{7.18}$$

We will use the estimates (7.8)–(7.18) later.

8. Physical invariant measure

Here we construct a natural ('physical') $\mathcal{F}_\varepsilon$-invariant measure on $\mathcal{M}$ that attracts Lebesgue a.e. point $X \in \mathcal{M}$.

Recall that the basin of attraction B_ν of an ergodic $\mathcal{F}_\varepsilon$-invariant measure ν is the set of points $X \in \mathcal{M}$ such that

$$\frac{1}{n}\big[f(X) + f(\mathcal{F}_\varepsilon(X)) + \cdots + f(\mathcal{F}_\varepsilon^{n-1}(X))\big] \to \int_{\mathcal{M}} f\, d\nu$$

for every bounded continuous function f. By the ergodic theorem, $\nu(B_\nu) = 1$. We say that ν is a *physical* measure if $\mathrm{Leb}(B_\nu) > 0$, i.e. there is a positive chance of 'seeing' this measure in a physical experiment where one observes an orbit of a randomly selected point $X \in \mathcal{M}$.

In hyperbolic systems like ours, the basin B_ν of every measure ν is (mod 0) a union of stable manifolds. Thus the condition $\mathrm{Leb}(B_\nu) > 0$ is equivalent to $m_W(W \cap B_\nu) > 0$ for some unstable curve W. It is then natural to construct a physical measure by iterating the Lebesgue measure m_W defined on an unstable curve, i.e. by taking a Cesaro limit point of the sequence of its images $\mathcal{F}_\varepsilon^n(m_W)$.

Suppose we start with a standard pair ℓ_0 (or more generally, with a standard family $\mathcal{G}_0$ that has a finite $\mathcal{Z}_{\mathcal{G}_0} < \infty$). Then we consider the sequence of measures $\mathbb{P}_{\mathcal{G}_n} = \mathcal{F}_\varepsilon^n(\mathbb{P}_{\mathcal{G}_0})$. For all $n \ge n_0 \sim C|\ln \mathcal{Z}_{\mathcal{G}_0}|$, the measure $\mathbb{P}_{\mathcal{G}_n}$ will be supported on a *proper* standard family $\mathcal{G}_n$. As such, it will be mostly supported on long unstable curves. More precisely, for any $\zeta > 0$ we have

$$\mathbb{P}_{\mathcal{G}_n}\big(\cup_{W_\alpha \in \mathcal{G}_n\colon |W_\alpha| < \zeta} W_\alpha\big) \le C\zeta \tag{8.1}$$

for some constant $C > 0$.

Next, for any $\zeta > 0$, consider the class $\mathcal{C}_u(\zeta)$ of unstable curves $W \subset \mathcal{M}$ of length $\ge \zeta$. Denote by $\overline{\mathcal{C}_u(\zeta)}$ its closure in the Hausdorff metric. Recall that our unstable curves are C^2 with uniformly bounded curvature, and their tangent vectors satisfy (4.1). Therefore ([17, Lemma 4.60]) all the curves in the class $\overline{\mathcal{C}_u(\zeta)}$ are of length $\ge \zeta$, they are at least C^1 (but not necessarily C^2, though their derivatives are Lipschitz continuous), and their tangent vectors also satisfy (4.1). We will call curves $W \in \cup_{\zeta>0}\overline{\mathcal{C}_u(\zeta)}$ *generalized unstable curves*. Accordingly, we define generalized standard pairs and families as those supported on generalized unstable curves. (For brevity, we will omit the word 'generalized' most of the time.)

Proposition 8.1. *For every generalized standard family $\mathcal{G}$ the sequence of Cesaro averages of the images $\mathcal{F}_\varepsilon^n(\mathbb{P}_{\mathcal{G}})$ has a weakly convergent subsequence. The limit measure ν_ε will be $\mathcal{F}_\varepsilon$-invariant, and it will be supported on a proper generalized standard family $\mathcal{G}_\varepsilon$.*

Proof. Our argument is similar to that used in [1] for construction of physical measures for partially hyperbolic diffeomorphisms. First we define a metric on the space of all generalized standard pairs. Given two pairs $\ell_1 = (W_1, \rho_1)$ and $\ell_2 = (W_2, \rho_2)$, we parameterize W_1 and W_2 by a normalized arclength parameter s, i.e. $W_1 = \{r_1(s), \varphi_1(s)\}$ and $W_2 = \{r_2(s), \varphi_2(s)\}$ for $0 \le s \le 1$. We assume that the orientations of these parameterizations agree – for example, $s = 0$ corresponds to the bottom left endpoint and $s = 1$ to the top right endpoint of each curve (recall that the curves are monotonically

increasing in the $r\varphi$ coordinates, i.e. they run from bottom left to top right). The metric is now defined as

$$\operatorname{dist}(\ell_1, \ell_2) = \max_{0 \le s \le 1} \{|r_1(s) - r_2(s)|, |\varphi_1(s) - \varphi_2(s)|, |\rho_1(s) - \rho_2(s)|\}.$$

For any $\zeta > 0$ we denote by Ψ_ζ the metric space of standard pairs supported on unstable curves of length $\ge \zeta$. Observe that this space is compact. Now any standard family $\mathcal{G}$ is a measure on $\cup_{\zeta>0}\Psi_\zeta$, we denote that measure by $\tilde{\mathbb{P}}_\mathcal{G}$ (note that it is different from $\mathbb{P}_\mathcal{G}$, as it is defined on the space of standard pairs, while $\mathbb{P}_\mathcal{G}$ is defined on $\mathcal{M}$).

Now let $\{\mathcal{G}_i\}$ be any sequence of proper standard families, then

$$\inf_i \tilde{\mathbb{P}}_{\mathcal{G}_i}(\Psi_\zeta) \to 1 \qquad \text{as} \quad \zeta \to 0,$$

due to (8.1). Thus, the sequence $\tilde{\mathbb{P}}_{\mathcal{G}_i}$ has a weakly convergent subsequence.

Now let $\mathcal{G}$ be any standard family with $\mathcal{Z}_\mathcal{G} < \infty$. Then for all $n \ge n_\mathcal{G}$ the image $\mathcal{F}_\varepsilon^n(\tilde{\mathbb{P}}_\mathcal{G})$ will be a proper standard family. Due to the above, its Cesaro averages will have a weak limit point, which will be supported on a proper standard family, we denote it by $\mathcal{G}_\varepsilon$. It will obviously be invariant under $\mathcal{F}_\varepsilon$, and its projection onto $\mathcal{M}$ will be an $\mathcal{F}_\varepsilon$-invariant probability measure ν_ε. □

We will show later that the physical measure ν_ε is unique, ergodic, and mixing.

Next we investigate the support of the so defined measure $\tilde{\mathbb{P}}_{\mathcal{G}_\varepsilon}$. We say that a standard pair $\ell = (W, \rho)$ belongs in the support of $\tilde{\mathbb{P}}_{\mathcal{G}_\varepsilon}$ if for any $\delta > 0$ the measure of the δ-neighborhood of ℓ is positive. The δ-neighborhood consists of standard pairs on unstable curves W' of length $|W'| \ge |W| - 4\delta$ that are δ-close to W. Since $\tilde{\mathbb{P}}_{\mathcal{G}_\varepsilon}$ is invariant, we see that (at least some of) the curves W' are images of other unstable curves (or components thereof). By continuity, W is an image of an unstable curve, too, we will call it W_{-1}. In other words, at least one branch of $\mathcal{F}_\varepsilon^{-1}$ is defined and continuous on W, and it takes W to the unstable curve W_{-1} (of course, W_{-1} will be shorter than W). In that case W_{-1} belongs to the support of ν_ε as well.

We say that an unstable curve $W_0 \subset \mathcal{M}$ is an *unstable manifold* if there is a sequence of unstable curves W_{-i} such that $\mathcal{F}_\varepsilon(W_{-i-1}) = W_{-i}$ for all $i \ge 0$. Our previous analysis implies

Proposition 8.2. *The proper generalized standard family $\mathbb{P}_{\mathcal{G}_\varepsilon}$ constructed above and corresponding to the invariant measure ν_ε consists of unstable manifolds. In other words, ν_ε is supported on a union of unstable manifolds.*

In this sense, our invariant measure ν_ε is an analogue of Sinai-Ruelle-Bowen (SRB) measures for hyperbolic systems – it is absolutely continuous on unstable manifolds and ergodic (see below). (We note, however, that the measure ν_ε can be represented by many different generalized standard families, not all of them consisting of unstable manifolds.)

We also note that our unstable manifolds *do not* foliate $\mathcal{M}$, in fact they may cross each other (because our map $\mathcal{F}_\varepsilon$ is not invertible). One can think of $\mathbb{P}_{\mathcal{G}_\varepsilon}$ as a family of unstable manifolds that are 'scattered' all over

$\mathcal{M}$ with plenty of mutual intersections. Their distribution in $\mathcal{M}$ may be very inhomogeneous, i.e. they may 'pile up' in some places and completely avoid other places (in fact their union may possibly be nowhere dense in $\mathcal{M}$).

The above proposition is included here for the purpose of comparing our invariant measure ν_ε with "usual" SRB states; our further analysis will not rely on it.

Next we turn to the Coupling Lemma. This is a useful tool in the studies of hyperbolic maps; and it is flexible enough to be applied to non-invertible maps like ours.

We briefly describe the relevant constructions, see a detailed exposition in [17, Section 7.5] and [12, Appendix A]. First, every standard pair $\ell = (W, \rho)$ is replaced with a 'rectangle' $\hat{W} := W \times [0,1]$ equipped with a probability measure $\hat{\mathbb{P}}_\ell$ defined by

$$d\hat{\mathbb{P}}_\ell(X,t) = d\mathbb{P}_\ell(X)\,dt = \rho(X)\,dX\,dt, \tag{8.2}$$

i.e. the density of $\hat{\mathbb{P}}_\ell$ is also ρ. The map $\mathcal{F}_\varepsilon^n$ can be naturally defined on 'rectangles' $\hat{W}$ by $\mathcal{F}_\varepsilon^n(X,t) = (\mathcal{F}_\varepsilon^n X, t)$.

Given a standard family $\mathcal{G} = (W_\alpha, \rho_\alpha)$, $\alpha \in \mathfrak{A}$, with a factor measure $\lambda_\mathcal{G}$, we denote by $\hat{\mathcal{G}} = (\hat{W}_\alpha, \rho_\alpha)$ the family of the corresponding rectangles equipped with the same factor measure $\lambda_\mathcal{G}$, and denote by $\hat{\mu}_\mathcal{G}$ the induced measure on the union $\cup_\alpha \hat{W}_\alpha$.

Lemma 8.3 (Coupling Lemma). *Let $\mathcal{G} = (W_\alpha, \rho_\alpha)$, $\alpha \in \mathfrak{A}$, and $\mathcal{E} = (W_\beta, \rho_\beta)$, $\beta \in \mathfrak{B}$, be two proper standard families. Then there exist a bijection (a coupling map) $\Theta\colon \cup_\alpha \hat{W}_\alpha \to \cup_\beta \hat{W}_\beta$ that preserves measure; i.e. $\Theta(\hat{\mu}_\mathcal{G}) = \hat{\mu}_\mathcal{E}$, and a (coupling time) function $\Upsilon : \cup_\alpha \hat{W}_\alpha \to \mathbb{N}$ such that two properties hold:*

A. *Let $(X,t) \in \hat{W}_\alpha$, $\alpha \in \mathfrak{A}$, and $\Theta(X,t) = (Y,s) \in \hat{W}_\beta$, $\beta \in \mathfrak{B}$. Then the points $\mathcal{F}_\varepsilon^m(X)$ and $\mathcal{F}_\varepsilon^m(Y)$ lie on the same stable manifold $W^s \subset \mathcal{M}$ for $m = \Upsilon(X,t)$.*

B. *There is a uniform exponential tail bound on the function Υ:*

$$\hat{\mu}_\mathcal{G}\big(\Upsilon > n\big) \le C_\Upsilon \vartheta_\Upsilon^n, \tag{8.3}$$

for some constants $C_\Upsilon = C_\Upsilon(\mathcal{D}) > 0$ and $\vartheta_\Upsilon = \vartheta_\Upsilon(\mathcal{D}) < 1$.

We emphasize that the constants C_Υ and ϑ_Υ are uniform in ε.

Proof The argument goes along the same lines as in [17, Section 7.5] and [12, Appendix A] (we have already prepared all the necessary technical tools). The only new issue is the uniformity in ε. To settle it, we recall that the proof uses a quadrilateral $R \subset \mathcal{M}$ bounded by two stable curves and two unstable curves (called a 'rhombus' in [17]) where the coupling is defined explicitly (R contains all the points $\mathcal{F}_\varepsilon^m(X)$ and $\mathcal{F}_\varepsilon^m(Y)$ mentioned in part A). That rhombus must first be constructed for the billiard map $\mathcal{F}_0$, and then, because $\mathcal{F}_\varepsilon$ is a small perturbation of $\mathcal{F}_0$, the rhombus R will have nearly the same properties for all small ε. In particular the fact that there exists m_0 such that for any proper unstable curve $\mathcal{F}_\varepsilon^{m_0} W \bigcap R \neq \emptyset$ is first proven for $\varepsilon = 0$ using mixing of $\mathcal{F}_0$ and then extended to $\varepsilon \neq 0$ using compactness of the set of

proper unstable curves. This perturbative argument is described in detail in [9, pp. 229–233], and it works in our case as well. □

Remark. The above perturbative argument puts severe restrictions on ε, i.e. it works only for *very* small ε; see a remark on page 232 in [9] for explanations and related issues. One can expect that hyperbolicity, regularity conditions, and the existence of physical measures hold for reasonably small ε, but the uniqueness and strong statistical properties (see below) hold only for extremely small ε. We expect that if we increase ε continuously, one first observes a unique physical measure, then a finite collection of physical (SRB-like) measures, and then singular non-SRB stationary states. For models with Gaussian thermostats numerical experiments of this sort were done in [21].

In plain words, the Coupling Lemma means that the images of any two measures supported on proper standard families will get close together (exponentially fast), and their further images will become almost indistinguishable. In particular, one of the two standard families in Lemma 8.3 can be $\mathcal{G}_\varepsilon$ supporting the invariant measure $\nu_\varepsilon = \mathbb{P}_{\mathcal{G}_\varepsilon}$; then the images of any other measure $\mathbb{P}_\mathcal{G}$ converge to ν_ε exponentially fast (in the sense specified by the coupling map).

Corollary 8.4. *The measure $\nu_\varepsilon = \mathbb{P}_{\mathcal{G}_\varepsilon}$ described in Proposition* 8.1 *is unique and independent from the initial standard family $\mathcal{G}$. It is ergodic and mixing. In addition, we have the following weak limit*

$$\lim_{n\to\infty} \mathcal{F}_\varepsilon^n\big(\mathbb{P}_\mathcal{G}\big) = \nu_\varepsilon \tag{8.4}$$

for any standard family $\mathcal{G}$ with a finite $\mathcal{Z}_\mathcal{G} < \infty$.

Note that $\mathbb{P}_\mathcal{G}$ in (8.4) can be replaced with ν_0, as one can foliate $\mathcal{M}$ by unstable curves and condition the measure ν_0 on them to get a $\mathbb{P}_\mathcal{G}$.

Proof. The uniqueness and ergodicity readily follow from the Coupling Lemma, and so does (8.4). To show that ν_ε is mixing it is enough to verify that

$$\lim_{n\to\infty} \nu_\varepsilon\big(f\cdot(g\circ\mathcal{F}_\varepsilon^n)\big) = \nu_\varepsilon(f)\nu_\varepsilon(g) \tag{8.5}$$

for any continuous functions f, g on $\mathcal{M}$. Clearly, f and g can be approximated by smooth functions, then f can be replaced with a linear combination of smooth functions with values in the interval $[1-\delta_0, 1+\delta_0]$ for a small $\delta_0 > 0$ and mean values $=1$, and then $f\mathbb{P}_{\mathcal{G}_\varepsilon}$ will be a proper standard family; thus (8.5) follows from (8.4). □

Now we address the statistical properties of the system $(\mathcal{M}, \mathcal{F}_\varepsilon, \nu_\varepsilon)$. We say that a function $f\colon \mathcal{M}\to\mathbb{R}$ is *dynamically Hölder continuous* if there are $\vartheta_f \in (0,1)$ and $K_f > 0$ such that for any $X, Y \in W$ lying on one unstable curve W

$$|f(X) - f(Y)| \le K_f \vartheta_f^{\mathbf{s}_+(X,Y)} \tag{8.6}$$

and for any $X, Y \in W^s$ lying on one stable manifold W^s

$$|f(X) - f(Y)| \le K_f \vartheta_f^{\mathbf{s}_-(X,Y)}, \tag{8.7}$$

where $\mathbf{s}_-(X,Y)$ is the largest $m \geq 0$ such that $W^s = \mathcal{F}_\varepsilon^m(W_1^s)$ for another stable manifold W_1^s. The value $\mathbf{s}_+(X,Y)$ is called the future separation time for the points X and Y, and we can naturally call $\mathbf{s}_-(X,Y)$ the past separation time.

We denote the space of such functions by $\mathcal{H}$. It contains every piecewise Hölder continuous function whose discontinuities coincide with those of $\mathcal{F}_\varepsilon^m$ for some $m > 0$. For example, the components $\Delta_{\varepsilon,x}, \Delta_{\varepsilon,y}$ of the vector displacement function $\mathbf{\Delta}_\varepsilon$ belong in $\mathcal{H}$ (to be proven in Section 10).

The following two propositions follow from the Coupling Lemma; see the proofs of Theorems 7.31 and 7.37 in [17].

Proposition 8.5 (Equidistribution). *Let $\mathcal{G}$ be a proper standard family. For any dynamically Hölder continuous function $f \in \mathcal{H}$ and $n \geq 0$*

$$\left| \int_{\mathcal{M}} f \circ \mathcal{F}_\varepsilon^n \, d\mathbb{P}_{\mathcal{G}} - \int_{\mathcal{M}} f \, d\nu_\varepsilon \right| \leq B_f \theta_f^n \tag{8.8}$$

where $B_f = 2C\big(K_f + \|f\|_\infty\big)$ and $\theta_f = \big[\max\{\vartheta_\Upsilon, \vartheta_f\}\big]^{1/2} < 1$; here $C > 0$ is a constant independent of $\mathcal{G}$ and ε.

In other words, iterations of measures on standard pairs weakly converge to the measure ν_ε, and the convergence is exponentially fast in the sense of (8.8).

Proposition 8.6 (Exponential bound on correlations). *For any pair of dynamically Hölder continuous functions $f, g \in \mathcal{H}$ and $n > 0$*

$$\big|\nu_\varepsilon\big(f \cdot (g \circ \mathcal{F}_\varepsilon^n)\big) - \nu_\varepsilon(f)\nu_\varepsilon(g)\big| \leq B_{f,g}\, \theta_{f,g}^n \tag{8.9}$$

where

$$\theta_{f,g} = \big[\max\big\{\vartheta_\Upsilon, \vartheta_f, \vartheta_g, e^{-1/c_3}\big\}\big]^{1/4} < 1,$$

where $c_3 > 0$ is the constant from Lemma 7.2, and

$$B_{f,g} = C\big(K_f \|g\|_\infty + K_g \|f\|_\infty + \|f\|_\infty \|g\|_\infty\big).$$

Remark. The invariant measure ν_ε in (8.9) can be replaced with any measure $\mathbb{P}_{\mathcal{G}}$ supported on a proper standard family (in particular, by the $\mathcal{F}_0$-invariant measure ν_0). In that case (8.9) takes form

$$\big|\mathbb{P}_{\mathcal{G}}\big(f \cdot (g \circ \mathcal{F}_\varepsilon^n)\big) - \mathbb{P}_{\mathcal{G}}(f)\nu_\varepsilon(g)\big| \leq B_{f,g}\, \theta_{f,g}^n.$$

The proof of this is just a simple adaptation of the standard proof of the above theorem, see e.g. the proof of Theorem 7.37 in [17]. This fact was used in [15].

The last theorem can be extended to multiple correlations and it implies, via a standard argument, Central Limit Theorem for the map $\mathcal{F}_\varepsilon$, see [17, Chapter 7] and [11].

Lastly we derive the Kawasaki-type formula for any dynamically Hölder continuous function $f \in \mathcal{H}$. Due to (8.4)

$$\nu_\varepsilon(f) = \nu_0(f) + \lim_{n\to\infty} \sum_{k=1}^{n} \nu_0\big[(f \circ \mathcal{F}_\varepsilon^k) - (f \circ \mathcal{F}_\varepsilon^{k-1})\big]. \tag{8.10}$$

Also recall that $\nu_0 = \mathbb{P}_{\mathcal{G}_0}$ for a proper standard family $\mathcal{G}_0$. Thus, due to Equidistribution property, $\nu_0(f \circ \mathcal{F}_\varepsilon^k)$ converges to $\nu_\varepsilon(f)$ exponentially fast. Therefore the series in (8.10) converges at an exponential rate, and we have the following tail bound:

$$\left| \sum_{k=n}^{\infty} \nu_0\big[(f \circ \mathcal{F}_\varepsilon^k) - (f \circ \mathcal{F}_\varepsilon^{k-1})\big] \right| \le 2B_f \theta_f^n / (1-\theta_f). \tag{8.11}$$

We note that if the Hölder exponent ϑ_f of the function f, its Hölder norm K_f, and its ∞-norm $\|f\|_\infty$ are all independent of ε, then the above estimate is uniform in ε, too.

9. Electrical current

Now we turn to the physically interesting feature – electrical current. In this section we present our arguments in a relatively general way suppressing some model-specific details; the latter will be supplied in the next section.

We first investigate the discrete-time current defined by

$$\hat{\mathbf{J}} = \lim_{n\to\infty} \tfrac{1}{n}\, \tilde{\mathbf{q}}_n = \nu_\varepsilon(\mathbf{\Delta}_\varepsilon),$$

where $\mathbf{\Delta}_\varepsilon = (\Delta_{\varepsilon,x}, \Delta_{\varepsilon,y}) = \tilde{\mathbf{q}}_1 - \mathbf{q}$ denotes the displacement vector, cf. (2.3). We write Δ_ε for both components $\Delta_{\varepsilon,x}$ and $\Delta_{\varepsilon,y}$ of $\mathbf{\Delta}_\varepsilon$. The function Δ_ε is bounded and dynamically Hölder continuous (see Corollary 10.4), hence the Kawasaki formula (8.10) applies:

$$\nu_\varepsilon(\Delta_\varepsilon) = \nu_0(\Delta_\varepsilon) + \sum_{n=1}^{\infty} \nu_0\big[(\Delta_\varepsilon \circ \mathcal{F}_\varepsilon^n) - (\Delta_\varepsilon \circ \mathcal{F}_\varepsilon^{n-1})\big], \tag{9.1}$$

in which the series converges exponentially. In fact, its Hölder exponent $\theta_{\Delta_\varepsilon} \in (0,1)$ is independent of ε and its norm is $K_{\Delta_\varepsilon} = \mathcal{O}(\varepsilon^{-a})$ with some constant $a > 0$ (see Corollary 10.4). Due to (8.11) we can choose $N = L|\ln\varepsilon|$ with a large constant $L > 0$ and rewrite (9.1) as

$$\nu_\varepsilon(\Delta_\varepsilon) = \nu_0(\Delta_\varepsilon) + \sum_{n=1}^{N} \nu_0\big[(\Delta_\varepsilon \circ \mathcal{F}_\varepsilon^n) - (\Delta_\varepsilon \circ \mathcal{F}_\varepsilon^{n-1})\big] + \chi_1, \tag{9.2}$$

where $\chi_1 = \mathcal{O}(\varepsilon^2)$. Here and in what follows we will denote by $\chi_1, \chi_2, \dots$ various remainder terms, they will all satisfy $\chi_i = \mathcal{O}(\varepsilon^{1+a_i})$ for some $a_i > 0$. Now let

$$\mathcal{M} = \cup_{k=0}^{\infty} M_k,$$

where M_k consists of points with exactly k preimages under $\mathcal{F}_\varepsilon^{-1}$. In other words, M_k consists of points where exactly k domains $\mathcal{M}_i^-$ (described in Section 5) overlap. (In fact, all $M_k \ne \emptyset$ only for $k \le k_0$, with some k_0 independent of ε.)

The set M_1 is overwhelmingly large, and we denote its complement by $M_\diamond = \mathcal{M} \setminus M_1$. In the finite horizon case, $\nu(M_\diamond) = \mathcal{O}(\varepsilon^2)$, and in the infinite horizon case $\nu_0(M_\diamond) = \mathcal{O}(\varepsilon^{3/2})$ due to (6.3). The inverse map $\mathcal{F}_\varepsilon^{-1}$ is uniquely defined on M_1, and we put $M_1^- = \mathcal{F}_\varepsilon^{-1}(M_1)$ and $M_\diamond^- = \mathcal{M} \setminus M_1^-$.

We also split $\nu_0 = \nu_{01} + \nu_{0\diamond}$, where ν_{01} denotes ν_0 restricted to M_1 and $\nu_{0\diamond}$ is ν_0 restricted to $M_\diamond$. Now the measure $\nu_{01}^- = \mathcal{F}_\varepsilon^{-1}(\nu_{01})$ is supported on M_1^-, and according to Lemma 4.3, for any $X \in M_1^-$ we have

$$\frac{d\nu_{01}^-}{d\nu_0}(X) = \frac{v}{v_1} = \sqrt{\frac{1+2\varepsilon x}{1+2\varepsilon x + 2\varepsilon\Delta_{\varepsilon,x}}} \tag{9.3}$$

(using the notation of Section 3). Now Taylor expansion gives

$$v/v_1 = 1 - \varepsilon\Delta_{\varepsilon,x} + \varepsilon\mathcal{R}_\varepsilon,$$

where $\mathcal{R}_\varepsilon$ is the remainder, whose contribution in the end will be negligible (see discussion after (10.7)). Let $\nu_{0\diamond}^-$ denote the measure on $M_\diamond^- = \mathcal{M} \setminus M_1^-$ having the same density v/v_1 as the measure ν_{01}^- on M_1^-. Note that $\nu_{01}^- + \nu_{0\diamond}^-$ is not necessarily a probability measure, in fact we have

$$\int_{\mathcal{M}} \frac{v}{v_1}\, d\nu_0 = \sum_{k=1}^{\infty} k\nu_0(M_k) = 1 - \chi_3$$

where $\chi_3 = \mathcal{O}(\varepsilon^{3/2})$. Normalizing $\nu_{01}^- + \nu_{0\diamond}^-$ gives a probability measure $\tilde{\mu}_0$ on $\mathcal{M}$ with density

$$g(X) = \frac{d\tilde{\mu}_0}{d\nu_0} = \frac{v}{v_1(1-\chi_3)} = 1 - \varepsilon\Delta_{\varepsilon,x} + \varepsilon\mathcal{R}_\varepsilon + \chi_4, \tag{9.4}$$

where $\chi_4 = \mathcal{O}(\varepsilon^{3/2})$. Summarizing our formulas, we obtain for every $n \geq 1$

$$\nu_0(\Delta_\varepsilon \circ \mathcal{F}_\varepsilon^{n-1}) = \tilde{\mu}_0(\Delta_\varepsilon \circ \mathcal{F}_\varepsilon^n) + \chi_{5,n}, \tag{9.5}$$

where

$$\begin{aligned}\chi_{5,n} &= \nu_{0\diamond}(\Delta_\varepsilon \circ \mathcal{F}_\varepsilon^{n-1}) - \nu_{0\diamond}^-(\Delta_\varepsilon \circ \mathcal{F}_\varepsilon^n) - \chi_3\, \tilde{\mu}_0(\Delta_\varepsilon \circ \mathcal{F}_\varepsilon^n) \\ &= \mathcal{O}(\varepsilon^{5/4}|\ln\varepsilon|) + \mathcal{O}(\varepsilon^{3/2}|\ln\varepsilon|)\end{aligned}$$

(here we used (7.11) and (7.13)). Now the Kawasaki formula (9.2) can be rewritten as

$$\nu_\varepsilon(\Delta_\varepsilon) = \nu_0(\Delta_\varepsilon) + \sum_{n=1}^{N} \nu_0\big[(1-g)(\Delta_\varepsilon \circ \mathcal{F}_\varepsilon^n)\big] + \chi_5, \tag{9.6}$$

where

$$\chi_5 = \sum_{n=1}^{N} \chi_{5,n} = \mathcal{O}\big(\varepsilon^{5/4}|\ln\varepsilon|^2\big).$$

Next we observe that

$$\nu_0(g\Delta_\varepsilon) = \frac{1}{1-\chi_3}\int_{M_1^-} \frac{v}{v_1}\,\Delta_\varepsilon\, d\nu_0 + \frac{1}{1-\chi_3}\int_{M_\diamond^-} \frac{v}{v_1}\,\Delta_\varepsilon\, d\nu_0 \tag{9.7}$$

and note that the integral $I\colon = \int_{M_\diamond^-} \Delta_\varepsilon\, d\nu_0$ is $\mathcal{O}(\varepsilon^2)$ for systems with finite horizon, but $I = \mathcal{O}(\varepsilon)$ for systems with infinite horizon; recall (7.18). Now we define a new function

$$\Delta_\varepsilon^- = \begin{cases} \Delta_\varepsilon \circ \mathcal{F}_\varepsilon^{-1} & \text{on } M_1 \\ 0 & \text{on } M_\diamond \end{cases} \tag{9.8}$$

and rewrite (9.7) as

$$\begin{aligned}\nu_0(g\Delta_\varepsilon) &= \frac{1}{1-\chi_3}\int_{M_1}\Delta_\varepsilon^-\,d\nu_0 + I + \chi_6\\ &= \nu_0(\Delta_\varepsilon^-) + I + \chi_7,\end{aligned} \tag{9.9}$$

where χ_6 and χ_7 are $\mathcal{O}(\varepsilon^{3/2})$. Therefore

$$\nu_0(\Delta_\varepsilon) = \nu_0(\Delta_\varepsilon^-) + \nu_0\big[(1-g)\Delta_\varepsilon\big] + I + \chi_7$$

and so

$$\nu_0(\Delta_\varepsilon) = \tfrac{1}{2}\left[\nu_0(\Delta_\varepsilon) + \nu_0(\Delta_\varepsilon^-)\right] + \tfrac{1}{2}\,\nu_0\big[(1-g)\Delta_\varepsilon\big] + I/2 + \chi_7/2.$$

We will show that $\nu_0(\Delta_\varepsilon) + \nu_0(\Delta_\varepsilon^-) = \mathcal{O}(\varepsilon^a)$, where $a = 2$ for systems with finite horizon and $a = 1$ for systems with infinite horizon (Lemma 10.1).

Combining all our formulas gives

$$\nu_\varepsilon(\Delta_\varepsilon) = \tfrac{1}{2}\,\nu_0\big[(1-g)\Delta_\varepsilon\big] + \sum_{n=1}^{N}\nu_0\big[(1-g)(\Delta_\varepsilon\circ\mathcal{F}_\varepsilon^n)\big] + \mathcal{O}(\varepsilon^a), \tag{9.10}$$

where $a > 1$ for systems with finite horizon and $a = 1$ for systems with infinite horizon. Using Taylor expansion (9.4) gives

$$\begin{aligned}\nu_\varepsilon(\Delta_\varepsilon) = {}& \tfrac{1}{2}\,\varepsilon\nu_0(\Delta_{\varepsilon,x}\Delta_\varepsilon) + \varepsilon\sum_{n=1}^{N}\nu_0\big[(\Delta_\varepsilon\circ\mathcal{F}_\varepsilon^n)\Delta_{\varepsilon,x}\big]\\ &- \tfrac{1}{2}\,\varepsilon\nu_0(\mathcal{R}_\varepsilon\Delta_\varepsilon) - \varepsilon\sum_{n=1}^{N}\nu_0\big[(\Delta_\varepsilon\circ\mathcal{F}_\varepsilon^n)\mathcal{R}_\varepsilon\big] + \mathcal{O}(\varepsilon^a).\end{aligned} \tag{9.11}$$

The contribution of the remainder $\mathcal{R}_\varepsilon$ is small and can be incorporated into the last term $\mathcal{O}(\varepsilon^a)$. The correlations $\nu_0\big[\Delta_{\varepsilon,x}(\Delta_\varepsilon\circ\mathcal{F}_\varepsilon^n)\big]$ decay exponentially and uniformly in ε (see Proposition 10.6). The vector $\boldsymbol{\Delta}_\varepsilon = (\Delta_{\varepsilon,x}, \Delta_{\varepsilon,y})$ depends on ε continuously, so using *a priori* bounds of Lemma 10.2 we see that for every $n \ge 1$ we have

$$\lim_{\varepsilon\to 0}\nu_0\big[\Delta_{\varepsilon,x}(\Delta_\varepsilon\circ\mathcal{F}_\varepsilon^n)\big] = \nu_0\big[\Delta_{0,x}(\Delta_0\circ\mathcal{F}_0^n)\big], \tag{9.12}$$

where $\Delta_{0,x}$ and Δ_0 denote the components of the displacement vector $\boldsymbol{\Delta}_0$ in the field-free (billiard) dynamics. In the finite horizon case, (9.12) holds for $n = 0$ as well. Thus, in the finite horizon case we arrive at

$$\hat{\mathbf{J}} = \nu_\varepsilon(\boldsymbol{\Delta}_\varepsilon) = \tfrac{1}{2}\,\mathbf{D}\mathbf{E} + o(\varepsilon), \tag{9.13}$$

where $\mathbf{D}$ is the diffusion matrix (1.3).

In the infinite horizon case, the very first term in (9.11), i.e. $\frac{1}{2}\,\varepsilon\nu_0(\Delta_{\varepsilon,x}\Delta_\varepsilon)$ is dominant, it is $\mathcal{O}(\varepsilon|\ln\varepsilon|)$ due to (7.9). In fact, we will show in Section 10, see (10.12), that

$$\nu_0(\boldsymbol{\Delta}_\varepsilon\otimes\boldsymbol{\Delta}_\varepsilon) = |\log\varepsilon|\,\mathbf{D}_\infty + \mathcal{O}(1) \tag{9.14}$$

where $\mathbf{D}_\infty$ is the super-diffusion matrix (1.5) for the respective field-free (billiard) system. Therefore the current is given by

$$\hat{\mathbf{J}} = \nu_\varepsilon(\boldsymbol{\Delta}_\varepsilon) = \tfrac{1}{2}\,|\log\varepsilon|\,\mathbf{D}_\infty\mathbf{E} + \mathcal{O}(\varepsilon). \tag{9.15}$$

Next, basic facts from the theory of suspension flows (see [22, pp. 292–295], [5, pp. 21–22], or [17, Section 2.9]) readily give (2.3) and (2.7). Thus in order to complete the proofs of the main formulas (2.4) and (2.8) it suffices to show that, as stated in Theorems 6 and 7,

$$\bar{\tau}_\varepsilon = \bar{\tau} + \mathcal{O}(\varepsilon^a), \tag{9.16}$$

for some $a > 0$. This will be done in Section 10 (see Lemma 10.8).

It remains to prove the Central Limit Theorem and the corresponding formulas for the diffusion matrices, i.e. equations (2.5)-(2.6) and (2.9)-(2.10). According to general results, cf. [26] or [17, Theorem 7.68], the continuous-time CLT follows from its discrete-time counterpart whenever the corresponding ceiling function is bounded and dynamically Hölder continuous. Our ceiling function τ_ε has these properties, as we show in the next section.

Now the discrete-time CLT (mentioned in Section 8) says that

$$\frac{\tilde{\mathbf{q}}_n - n\hat{\mathbf{J}}}{\sqrt{n}} \Rightarrow \mathcal{N}(0, \hat{\mathbf{D}}^*_\varepsilon), \tag{9.17}$$

where the covariance matrix $\hat{\mathbf{D}}^*_\varepsilon$ is given by the sum of correlations

$$\begin{aligned}\hat{\mathbf{D}}^*_\varepsilon &= \nu_\varepsilon\big(\boldsymbol{\Delta}_\varepsilon \otimes \boldsymbol{\Delta}_\varepsilon\big) - \nu_\varepsilon(\boldsymbol{\Delta}_\varepsilon) \otimes \nu_\varepsilon(\boldsymbol{\Delta}_\varepsilon) \\ &\quad + 2\sum_{n=1}^{\infty}\Big(\nu_\varepsilon\big[(\boldsymbol{\Delta}_\varepsilon \circ \mathcal{F}^n_\varepsilon) \otimes \boldsymbol{\Delta}_\varepsilon\big] - \nu_\varepsilon(\boldsymbol{\Delta}_\varepsilon) \otimes \nu_\varepsilon(\boldsymbol{\Delta}_\varepsilon)\Big).\end{aligned} \tag{9.18}$$

The series in (9.18) converges exponentially fast, and we will show in the next section that the convergence is uniform in ε. We will also show (see Lemma 10.8) that, for each $n \geq 0$,

$$\nu_\varepsilon\big((\boldsymbol{\Delta}_\varepsilon \circ \mathcal{F}^n_\varepsilon) \otimes \boldsymbol{\Delta}_\varepsilon\big) = \nu_0\big((\boldsymbol{\Delta}_\varepsilon \circ \mathcal{F}^n_\varepsilon) \otimes \boldsymbol{\Delta}_\varepsilon\big) + \mathcal{O}(\varepsilon^a) \tag{9.19}$$

for some $a > 0$. (We also recall that $\nu_\varepsilon(\boldsymbol{\Delta}_\varepsilon)$ is small, according to (9.13) and (9.15).) This, along with (9.12) and (9.14), implies that

$$\hat{\mathbf{D}}^*_\varepsilon = \mathbf{D} + o(1)$$

for systems with finite horizon and

$$\hat{\mathbf{D}}^*_\varepsilon = |\log\varepsilon|\,\mathbf{D}_\infty + \mathcal{O}(1) \tag{9.20}$$

in the infinite horizon case. We also recall that $\mathbf{D}^*_\varepsilon = \bar{\tau}_\varepsilon^{-1}\hat{\mathbf{D}}^*_\varepsilon$ by a standard formula [17, Theorem 7.68]. This completes the proof of (2.5)-(2.6) and (2.9)-(2.10), and thus that of Theorems 6 and 7.

10. Finishing the proofs

Here we prove various technical statements made in Section 9. Our arguments mostly follow the lines of Sections 8–10 in [15] where Gaussian thermostatted Lorentz gases were treated. We sketch the steps that repeat those of [15] and give details whenever our arguments differ from those of [15], in particular when gaps and overlaps are involved.

Recall that Δ_ε denotes either component, $\Delta_{\varepsilon,x}$ or $\Delta_{\varepsilon,y}$, of the displacement vector $\mathbf{\Delta}_\varepsilon$. Our map $\mathcal{F}_\varepsilon$ is not invertible, but the function Δ_ε^- defined by (9.8) plays the role of $\Delta_\varepsilon \circ \mathcal{F}_\varepsilon^{-1}$.

Lemma 10.1. *We have $\nu_0(\Delta_\varepsilon) + \nu_0(\Delta_\varepsilon^-) = \mathcal{O}(\varepsilon^a)$, where $a = 2$ for systems with finite horizon and $a = 1$ for systems with infinite horizon.*

Proof. Let $X = (r, \varphi) \in M_1$ be a point such that we also have $\mathcal{I}(X) = (r, -\varphi) \in M_1$ (recall that $\mathcal{I}$ denotes the involution on $\mathcal{M}$). Since the density $\cos\varphi$ of the measure ν_0 is equal at the points X and $\mathcal{I}(X)$, we can combine them and estimate the following sum:

$$\Delta_\varepsilon(r,\varphi) + \Delta_\varepsilon^-(r,-\varphi) + \Delta_\varepsilon(r,-\varphi) + \Delta_\varepsilon^-(r,\varphi). \tag{10.1}$$

The key observation is that $\Delta_\varepsilon(r,\varphi)$ and $\Delta_\varepsilon^-(r,-\varphi)$ nearly cancel each other (and so do the other two terms). Indeed, they are projections (on the x or y axis) of two trajectories starting at the same point r, shooting at the same angle φ, but having slightly different initial velocities (according to the local time reversibility of our dynamics; see Section 5). In fact, the difference between their velocities is $\mathcal{O}(\varepsilon|\Delta_\varepsilon(X)|)$. Note that if the velocities were equal, then the trajectories would coincide, all the way up the next collision, and because they run in the opposite directions the first two terms in (10.1) would perfectly cancel out. But since the velocities differ a little, the trajectories run very closely, and the sum of the first two terms is (usually) small, see next.

An elementary analysis shows that when the above two trajectories cover the distance $|\Delta_\varepsilon(X)|$, i.e. when they are about to come to the next collision, they are $\mathcal{O}(\varepsilon^2|\Delta_\varepsilon(X)|^3)$ apart from each other. If they land on the same scatterer, at some angle φ_1, the landing points will be $\mathcal{O}(\varepsilon^2|\Delta_\varepsilon(X)|^3/\cos\varphi_1)$ apart. The overall contribution of such trajectories amounts to

$$J\colon = \nu_0\big(\varepsilon^2|\Delta_\varepsilon(X)|^3/\cos\varphi_1\big).$$

In the finite horizon case, $J = \mathcal{O}(\varepsilon^2)$. For infinite horizon,

$$J \asymp \varepsilon^2 \sum_m m^{0.5} + \varepsilon^2 m_L^{-3} \sum_m m^{3.5} = \mathcal{O}(\varepsilon^{5/4}).$$

If the above two trajectories land on different scatterers, then $\Delta_\varepsilon(r,\varphi) + \Delta_\varepsilon^-(r,-\varphi)$ is of order one, and we just need to estimate the measure of the set of such points X. Those points are characterized by the fact that their trajectories run $\mathcal{O}(\varepsilon^2 m^3)$-closely to the edge of a scatterer that is at distance $\asymp m$ away from X. Thus such points X are located in the $(\varepsilon^2 m^2)$-neighborhood of the borders of the cells $D_m^{(U)}$ and $D_m^{(L)}$ for all m. Thus such points make a set of measure

$$\sum_{m=1}^{m_U} \varepsilon^2 m^2 \big(1/\sqrt{m}\big)^2 + \sum_{m=1}^{m_L} \varepsilon^2 m^2 \big(\sqrt{m}/m_L\big)^2 = \mathcal{O}(\varepsilon).$$

It remains to account for points $X \in M_\diamond$ and $X \in \mathcal{I}^{-1}(M_\diamond)$. In the finite horizon case, they make a set of measure $\mathcal{O}(\varepsilon^2)$. For infinite horizon, we have

seen that $\int_{M_\diamond} \Delta_\varepsilon \, d\nu_0 = \mathcal{O}(\varepsilon^{5/4} |\ln \varepsilon|)$. A similar analysis for the set $\mathcal{I}^{-1}(M_\diamond)$ shows that

$$\int_{\mathcal{I}^{-1}(M_\diamond)} \Delta_\varepsilon \, d\nu_0 = \mathcal{O}(\varepsilon), \tag{10.2}$$

which is an analogue of (7.18). The lemma is proven. □

Lemma 10.2. *For each $n \ge 0$ we have*

$$(\mathcal{F}_\varepsilon^n \nu_0)\big(D_m^{(U)}\big) \asymp 1/m^3, \qquad (\mathcal{F}_\varepsilon^n \nu_0)\big(D_m^{(L)}\big) \asymp m/m_L^4 \tag{10.3}$$

and the same estimates hold for the limit measure ν_ε.

Proof. The proof is almost identical to that of Lemma 8.1 in [15]: for small n (say, for $n < \varepsilon^{-0.1}$), we use the fact that the (local) Jacobian (4.11) of the map $\mathcal{F}_\varepsilon$ is very close to one, hence the (local) Jacobian of $\mathcal{F}_\varepsilon^n$ is still close to one (it is enough for us that the Jacobian of $\mathcal{F}_\varepsilon^n$ is between 0.9 and 1.1). For larger n we use the equidistribution (Theorem 8.5): it shows that the sequence of the above measures converges exponentially fast, hence it will already be close to its limit when $n \ge \varepsilon^{-0.1}$.

In addition, now we need to estimate the effect of gaps and overlaps on the above measures for small n. Due to (7.16), the measure of gaps and overlaps that come to $D_m^{(U)}$ during the first n iterations is $\mathcal{O}(n\varepsilon^{5/4}/m^2)$ which is $o(1/m^3)$ for $n < \varepsilon^{-0.1}$. Similarly, due to (7.17), the measure of gaps and overlaps that come to $D_m^{(L)}$ during the first n iterations is $\mathcal{O}(n\varepsilon^{5/4}/m_L^2)$ which is $o(m/m_L^4)$ for $n < \varepsilon^{-0.1}$. □

Lemma 10.3. *Let $X, Y \in \mathcal{M}$ be two nearby points such that their trajectories in $\mathcal{D}$ land, at the next collision, on the same scatterer in $\mathbb{R}^2$. Then we have*

$$\|\boldsymbol{\Delta}_\varepsilon(X) - \boldsymbol{\Delta}_\varepsilon(Y)\| \le C\sqrt{\|\boldsymbol{\Delta}_\varepsilon(X)\| \cdot \operatorname{dist}(X,Y)},$$

where $C > 0$ is a constant independent of ε.

This is an analogue of Lemma 8.2 in [15]. Its proof is an elementary calculation, because the trajectories between collisions are parabolas; we leave the details to the reader.

Corollary 10.4. *$\boldsymbol{\Delta}_\varepsilon$ is a dynamically Hölder continuous function with Hölder exponent $\vartheta_{\boldsymbol{\Delta}_\varepsilon} = 1/2$ and Hölder constant $K_{\boldsymbol{\Delta}_\varepsilon} \asymp \|\boldsymbol{\Delta}_\varepsilon\|_\infty \asymp 1/\sqrt{\varepsilon}$.*

This proves the Kawasaki formula (9.1) with the error estimate

$$\left| \int_{\mathcal{M}} \Delta_\varepsilon \circ \mathcal{F}_\varepsilon^n \, d\nu_0 - \int_{\mathcal{M}} \Delta_\varepsilon \, d\nu_\varepsilon \right| \le C\varepsilon^{-1/2}\theta^n. \tag{10.4}$$

Furthermore, for every $k \ge 2$ we have $K_{\Delta_\varepsilon^k} + \|\Delta_\varepsilon^k\|_\infty \asymp \varepsilon^{-k/2}$, and so

$$\left| \int_{\mathcal{M}} \Delta_\varepsilon^k \circ \mathcal{F}_\varepsilon^n \, d\nu_0 - \int_{\mathcal{M}} \Delta_\varepsilon^k \, d\nu_\varepsilon \right| \le C\varepsilon^{-k/2}\theta^n. \tag{10.5}$$

For $k = 1$, we can get a uniform bound, independent of ε:

Proposition 10.5. *For some constants $C > 0$ and $\theta < 1$, independent of ε,*

$$\left| \int_{\mathcal{M}} \Delta_\varepsilon \circ \mathcal{F}_\varepsilon^n \, d\nu_0 - \int_{\mathcal{M}} \Delta_\varepsilon \, d\nu_\varepsilon \right| \le C\theta^n. \tag{10.6}$$

The proof repeats that of Proposition 8.3 in [15] verbatim. The uniform convergence here justifies our choice of $N = L|\ln\varepsilon|$ in (9.2).

Next we examine the remainder $\mathcal{R}_\varepsilon$: (9.3) implies

$$1 - \frac{v}{v_1} = \eta - \frac{1\cdot 3}{2!}\,\eta^2 + \frac{1\cdot 3\cdot 5}{3!}\,\eta^3 - \cdots$$

where $\eta = \frac{\varepsilon\Delta_{\varepsilon,x}}{1+2\varepsilon x}$, thus

$$\mathcal{R}_\varepsilon = \frac{2\varepsilon x\Delta_\varepsilon}{1+2\varepsilon x} + \frac{1\cdot 3}{2!}\cdot\frac{\varepsilon\Delta_\varepsilon^2}{(1+2\varepsilon x)^2} - \frac{1\cdot 3\cdot 5}{3!}\cdot\frac{\varepsilon^2\Delta_\varepsilon^3}{(1+2\varepsilon x)^3} + \cdots \tag{10.7}$$

This expansion is similar to (8.8) in [15]. One can easily see that $\mathcal{R}_\varepsilon$ is dynamically Hölder continuous with the same exponent and norm as the function $\Delta_{\varepsilon,x}$. Besides, $\mathcal{R}_\varepsilon$ is bounded (uniformly in ε), and $\mathcal{R}_\varepsilon \to 0$ pointwise, as $\varepsilon \to 0$. For all these reasons its contribution to (9.11) will be much easier to handle than that of $\Delta_{\varepsilon,x}$. In particular, $\nu_0(\mathcal{R}_\varepsilon\Delta_\varepsilon) = \mathcal{O}(\sqrt{\varepsilon})$, as the main contribution comes from the second term of (10.7), and we can apply (7.10) with $k = 3$.

Next we establish a uniform bound on correlations:

Proposition 10.6. *For some constants $C > 0$ and $\theta \in (0,1)$ independent of ε and all $n \ge 1$*

$$\left| \nu_\varepsilon\big[(\Delta_\varepsilon \circ \mathcal{F}_\varepsilon^n)\Delta_{\varepsilon,x}\big] - \nu_\varepsilon(\Delta_\varepsilon)\nu_\varepsilon(\Delta_{\varepsilon,x}) \right| \le C\theta^n \tag{10.8}$$

and

$$\left| \nu_0\big[(\Delta_\varepsilon \circ \mathcal{F}_\varepsilon^n)\Delta_{\varepsilon,x}\big] - \nu_\varepsilon(\Delta_\varepsilon)\nu_0(\Delta_{\varepsilon,x}) \right| \le C\theta^n \tag{10.9}$$

This is our analogue of Proposition 9.3 in [15], which in turn is an extension of the bounds on correlations in the infinite horizon Lorentz gas given in Proposition 9.1 in [15]. The proofs in [15] only use the estimates on the sizes, shapes, and measures of the cells $D_m^{(U)}$ and $D_m^{(L)}$, which are the same here, so they apply to the present situation without changes.

Proposition 10.6 implies

$$\nu_0\big[(\Delta_\varepsilon \circ \mathcal{F}_\varepsilon^n)\Delta_{\varepsilon,x}\big] = \nu_\varepsilon(\Delta_\varepsilon)\nu_0(\Delta_{\varepsilon,x}) + \mathcal{O}(\theta^n) \tag{10.10}$$

and similarly, replacing one Δ_ε with a much milder function $\mathcal{R}_\varepsilon$ we get

$$\nu_0\big[(\Delta_\varepsilon \circ \mathcal{F}_\varepsilon^n)\mathcal{R}_\varepsilon\big] = \nu_\varepsilon(\Delta_\varepsilon)\nu_0(\mathcal{R}_\varepsilon) + \mathcal{O}(\theta^n). \tag{10.11}$$

These uniform bounds and (9.11) imply our final results. Precisely, in the case of finite horizon they imply (9.13). For infinite horizon we obtain

$$\mathbf{J} = \nu_\varepsilon(\boldsymbol{\Delta}_\varepsilon) = \tfrac{1}{2}\,\varepsilon\nu_0(\boldsymbol{\Delta}_\varepsilon \otimes \boldsymbol{\Delta}_\varepsilon) + \mathcal{O}(\varepsilon),$$

so it remains to verify (9.14). This is done by direct integration, see below.

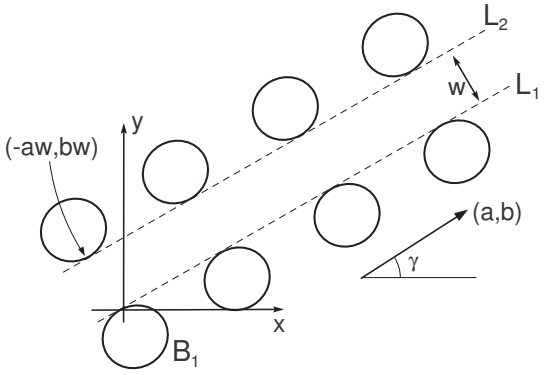

FIGURE 12. An infinite corridor bounded by two lines tangent to the scatterers.

First we note that the contribution from the lower cells $D_m^{(L)}$ is $\mathcal{O}(1)$, see the second sum in (7.9), hence they can be ignored. Second we can choose a large constant $C \gg 1$ and ignore all phase points with $\|\mathbf{\Delta}_\varepsilon\| \le C$. So we only consider trajectories that shoot from the initial scatterer facing an infinite corridor (see B_1 in Fig. 12) and landing on distant scatterers on the opposite side of that corridor (the upper row in Fig. 12).

Next, let L_1 and L_2 denote two parallel lines bordering our corridor, i.e. the two common tangent lines to all the scatterers along the corridor, see Fig. 12. Our trajectories leave the scatterer B_1, cross L_1 first, then after a long trip in the corridor they cross L_2 and land very shortly on the next scatterer in the top row. Let $\hat{\mathbf{\Delta}}_\varepsilon = (\hat{\Delta}_{\varepsilon,x}, \hat{\Delta}_{\varepsilon,y})$ denote the vector between the two crossing points, on L_1 and L_2 respectively. Note that $\Delta_{\varepsilon,x} = \hat{\Delta}_{\varepsilon,x} + \mathcal{O}(1)$ and $\Delta_{\varepsilon,y} = \hat{\Delta}_{\varepsilon,y} + \mathcal{O}(1)$, thus

$$\nu_0(\Delta_{\varepsilon,x}^2) = \nu_0(\hat{\Delta}_{\varepsilon,x}^2) + \mathcal{O}(1), \qquad \nu_0(\Delta_{\varepsilon,x}\Delta_{\varepsilon,y}) = \nu_0(\hat{\Delta}_{\varepsilon,x}\hat{\Delta}_{\varepsilon,y}) + \mathcal{O}(1),$$

and so we can replace $\Delta_{\varepsilon,x}, \Delta_{\varepsilon,y}$ with $\hat{\Delta}_{\varepsilon,x}, \hat{\Delta}_{\varepsilon,y}$.

Let γ denote the angle between the line L_1 and the field direction (i.e., the x axis). The equation of the line L_1 is $ay - bx = 0$, where $a = \cos\gamma$ and $b = \sin\gamma$, and that of the other line L_2 is $ay - bx = w$, where w denotes the width of the corridor.

Let $\mathbf{I} \subset L_1$ be a segment of L_1 between two consecutive scatterers, one of which is in $\mathcal{D}$, and let r be the arclength parameter on $\mathbf{I}$, so that $0 \le r \le r_{\max} = |\mathbf{I}|$. We regard $\mathbf{I}$ as an 'artificial' part of the boundary of our table $\tilde{\mathcal{D}}$, and then the measure ν_0 on it would be a smooth measure with density $c_\nu \cos\varphi \, dr \, d\varphi$, where φ is the angle made by the trajectory crossing $\mathbf{I}$ and the normal vector to L_1.

At every point $X_r = (x_r, y_r) \in \mathbf{I}$ we consider trajectories leaving X_r into the corridor, with velocity vector $\mathbf{v}$ such that $v = \|\mathbf{v}\| = \sqrt{1 + 2\varepsilon x_r}$

according to (2.1). Let $\psi = \pi/2 - \varphi$ denote the angle that $\mathbf{v}$ makes with the line L_1. There is a minimum $\psi_{\min} > 0$ so that the trajectory crosses L_2 before coming back to L_1. Let $(x_r + \hat{\Delta}_{\varepsilon,x}, y_r + \hat{\Delta}_{\varepsilon,y})$ denote the (first) intersection of our trajectory with L_2.

Proposition 10.7. *We have*

$$\int_0^{r_{\max}} \int_{\psi_{\min}}^{\pi/2} (\hat{\Delta}_{\varepsilon,x})^2 \sin\psi \, d\psi \, dr = \tfrac{1}{2} a^2 w^2 r_{\max} |\ln \varepsilon| + \mathcal{O}(1)$$

and

$$\int_0^{r_{\max}} \int_{\psi_{\min}}^{\pi/2} \hat{\Delta}_{\varepsilon,x} \hat{\Delta}_{\varepsilon,y} \sin\psi \, d\psi \, dr = \tfrac{1}{2} abw^2 r_{\max} |\ln \varepsilon| + \mathcal{O}(1).$$

This proposition easily implies

$$\nu_0(\mathbf{\Delta}_\varepsilon \otimes \mathbf{\Delta}_\varepsilon) = |\log \varepsilon| \, \mathbf{D}_\infty + \mathcal{O}(1) \tag{10.12}$$

see details in the proof of Eq. (10.5) in [15]. Note that $\sin\psi = \cos\varphi$.

Proof. This follows by an elementary calculation, we only outline the main steps. The initial velocity vector of the moving particle is $(v\cos(\gamma+\psi), v(\sin\gamma+\psi))$, and its position at time t is

$$\big(x_r + tv\cos(\gamma+\psi) + \tfrac{1}{2}\varepsilon t^2, y_r + tv\sin(\gamma+\psi)\big)$$

Substituting this into the equation $ay - bx = w$ of the line L_2 gives

$$\varepsilon b t^2 - 2tv\sin\psi + 2w = 0.$$

Solving this quadratic equation for $1/t$ gives the time of intersection of the trajectory with the line L_2:

$$t = \frac{2w}{v\sin\psi(1 + \sqrt{1 - 2\varepsilon bw/(v^2\sin^2\psi)})}$$

Incidentally, we see that $\psi_{\min} = \sin^{-1}\sqrt{2bw\varepsilon/v^2} \asymp \sqrt{\varepsilon}$. If we ignore small terms of order ε, we get

$$t \approx \frac{w}{v\sin\psi}, \qquad \hat{\Delta}_{\varepsilon,x} \approx \frac{aw}{\sin\psi}, \quad \hat{\Delta}_{\varepsilon,y} \approx \frac{bw}{\sin\psi}. \tag{10.13}$$

We note that

$$\int_{c\sqrt{\varepsilon}}^{C} \frac{d\psi}{\sin\psi} = \tfrac{1}{2}\,|\ln\varepsilon| + \mathcal{O}(1)$$

for any constants $c > 0$ and $0 < C < \pi/2$, thus the approximation (10.13) gives the right answer. To take care of terms of order ε we note that their contribution is of order

$$\int_{c\sqrt{\varepsilon}}^{C} \frac{\varepsilon d\psi}{\sin^2\psi} = \mathcal{O}(\sqrt{\varepsilon}),$$

thus they will not affect the final result. □

Lemma 10.8. *Formulas* (9.16) *and* (9.19) *hold.*

We prove (9.16) in two steps:

$$\nu_\varepsilon(\tau_\varepsilon) = \nu_0(\tau_\varepsilon) + \mathcal{O}(\varepsilon^a) \tag{10.14}$$

and

$$\nu_0(\tau_\varepsilon) = \nu_0(\tau_0) + \mathcal{O}(\varepsilon^a). \tag{10.15}$$

It is easy to verify directly that if a trajectory starts from a phase point $(\mathbf{q}, \mathbf{v}) \in \mathcal{M}$ and moves without collisions for a time τ, then it deviates from a billiard trajectory starting from the same phase point by $\mathcal{O}(\varepsilon\tau^2)$. Then the argument used in [15, Section 10] gives (10.15).

Now (10.14) and (9.19) are similar, except (10.14) applies to τ_ε and (9.19) applies to $(\boldsymbol{\Delta}_\varepsilon \circ \mathcal{F}_\varepsilon^n) \otimes \boldsymbol{\Delta}_\varepsilon$ for $n \ge 0$. One can check directly that the function τ_ε has all the same properties as $\boldsymbol{\Delta}_\varepsilon$ – it is dynamically Hölder continuous with exponent $\vartheta_{\tau_\varepsilon} \in (0,1)$ independent of ε and norm $K_f = \mathcal{O}(\varepsilon^{-a})$ for some $a > 0$, and it has the same order of magnitude as $\|\boldsymbol{\Delta}_\varepsilon\|$. Thus all of these estimates can be treated in the same way. We work out the most difficult of them, (9.19) for $n = 0$:

$$\nu_\varepsilon(\boldsymbol{\Delta}_\varepsilon \otimes \boldsymbol{\Delta}_\varepsilon) = \nu_0(\boldsymbol{\Delta}_\varepsilon \otimes \boldsymbol{\Delta}_\varepsilon) + \mathcal{O}(\varepsilon^a) \tag{10.16}$$

for some $a > 0$. To this end we apply the Kawasaki formula (9.1) to each component of the matrix

$$\boldsymbol{\Delta}_\varepsilon \otimes \boldsymbol{\Delta}_\varepsilon = \begin{bmatrix} \Delta_{\varepsilon,x}^2 & \Delta_{\varepsilon,x}\Delta_{\varepsilon,y} \\ \Delta_{\varepsilon,x}\Delta_{\varepsilon,y} & \Delta_{\varepsilon,y}^2 \end{bmatrix}.$$

They are treated similarly, and we only show the formulas for $\Delta_{\varepsilon,x}^2$:

$$\nu_\varepsilon(\Delta_{\varepsilon,x}^2) = \nu_0(\Delta_{\varepsilon,x}^2) + \sum_{n=1}^{\infty} \nu_0\big[(\Delta_{\varepsilon,x}^2 \circ \mathcal{F}_\varepsilon^n) - (\Delta_{\varepsilon,x}^2 \circ \mathcal{F}_\varepsilon^{n-1})\big], \tag{10.17}$$

in which the series converges exponentially. As we have shown, its Hölder exponent $\vartheta_{\Delta_{\varepsilon,x}^2} \in (0,1)$ is independent of ε and its norm is $K_{\Delta_{\varepsilon,x}^2} + \|\Delta_{\varepsilon,x}^2\|_\infty = \mathcal{O}(\varepsilon^{-1})$. Hence, due to (8.11), the terms of the above series are $\mathcal{O}(\varepsilon^{-1}\theta^n)$ for some constant $\theta \in (0,1)$. Thus we can choose $N = L|\ln\varepsilon|$ with a large constant $L > 0$ and rewrite (10.17) as

$$\nu_\varepsilon(\Delta_{\varepsilon,x}^2) = \nu_0(\Delta_{\varepsilon,x}^2) + \sum_{n=1}^{N} \nu_0\big[(\Delta_{\varepsilon,x}^2 \circ \mathcal{F}_\varepsilon^n) - (\Delta_{\varepsilon,x}^2 \circ \mathcal{F}_\varepsilon^{n-1})\big] + \mathcal{O}(\varepsilon). \tag{10.18}$$

Next we apply the analysis developed in Section 9 to the function $\Delta_{\varepsilon,x}^2$, instead of Δ_ε. In particular, an analogue of (9.5) will be

$$\nu_0(\Delta_{\varepsilon,x}^2 \circ \mathcal{F}_\varepsilon^{n-1}) = \tilde{\mu}_0(\Delta_{\varepsilon,x}^2 \circ \mathcal{F}_\varepsilon^n) + \chi_{9,n}, \tag{10.19}$$

where

$$\begin{aligned} \chi_{9,n} &= \nu_{0\diamond}(\Delta_{\varepsilon,x}^2 \circ \mathcal{F}_\varepsilon^{n-1}) - \nu_{0\diamond}^-(\Delta_{\varepsilon,x}^2 \circ \mathcal{F}_\varepsilon^n) - \chi_3\, \tilde{\mu}_0(\Delta_{\varepsilon,x}^2 \circ \mathcal{F}_\varepsilon^n) \\ &= \mathcal{O}(\varepsilon^{3/4}) + \mathcal{O}(\varepsilon) \end{aligned}$$

(here we used (7.12) and (7.14) with $k = 2$). Now the Kawasaki formula (10.18) can be rewritten as

$$\nu_\varepsilon(\Delta^2_{\varepsilon,x}) = \nu_0(\Delta^2_{\varepsilon,x}) + \sum_{n=1}^{N} \nu_0\big[(1-g)(\Delta^2_{\varepsilon,x} \circ \mathcal{F}^n_\varepsilon)\big] + \chi_9, \tag{10.20}$$

where

$$\chi_9 = \sum_{n=1}^{N} \chi_{9,n} = \mathcal{O}\big(\varepsilon^{3/4} |\ln \varepsilon|\big).$$

Using Taylor expansion (9.4) gives

$$\nu_\varepsilon(\Delta^2_{\varepsilon,x}) = \nu_0(\Delta^2_{\varepsilon,x}) + \varepsilon \sum_{n=1}^{N} \nu_0\big[(\Delta^2_{\varepsilon,x} \circ \mathcal{F}^n_\varepsilon)(\Delta_{\varepsilon,x} + \mathcal{R}_\varepsilon)\big] + \chi_{10}, \tag{10.21}$$

where the remainder is $\chi_{10} = \mathcal{O}(\varepsilon^{3/2} |\ln \varepsilon|^2)$ because $\chi_4 = \mathcal{O}(\varepsilon^{3/2})$ and $\nu_0(\Delta^2_{\varepsilon,x} \circ \mathcal{F}^n_\varepsilon) = \mathcal{O}(|\ln \varepsilon|)$ for every $n \ge 1$; see (7.9) and Lemma 10.2. Now using Hölder inequality gives

$$\big|\nu_0\big[(\Delta^2_{\varepsilon,x} \circ \mathcal{F}^n_\varepsilon)(\Delta_{\varepsilon,x} + \mathcal{R}_\varepsilon)\big]\big| \le \big[(\nu_0 \circ \mathcal{F}^n_\varepsilon)\big(|\Delta^3_{\varepsilon,x}|\big)\big]^{2/3} \big[\nu_0\big(|\Delta_{\varepsilon,x} + \mathcal{R}_\varepsilon|^3\big)\big]^{1/3},$$

and each of these integrals is bounded by

$$C \sum_{m=1}^{m_U} \frac{m^3}{m^3} + C \sum_{m=1}^{m_L} \frac{m^4}{m_L^4} \le C(m_U + m_L) \le C\varepsilon^{-1/2},$$

recall (7.10) for $k = 3$ and Lemma 10.2. Summing over $n \le L|\log \varepsilon|$ gives

$$\varepsilon \sum_{n=1}^{L|\log\varepsilon|} \nu_0\big[(\Delta^2_{\varepsilon,x} \circ \mathcal{F}^n_\varepsilon)(\Delta_{\varepsilon,x} + \mathcal{R}_\varepsilon)\big] = \mathcal{O}\big(\varepsilon^{1/2} |\log \varepsilon|\big),$$

which completes the proof of (10.16).

Appendix: The choice of a thermostat

In our model, we control the particle's kinetic energy indirectly, via dealing with its total energy; see Section 2. It might be tempting to control the kinetic energy directly, by resetting the speed of the particle to a constant value (say, to one) after every collision. Here we show that this would cause intractable complications.

Let us consider trajectories arriving at a fixed point (x_0, y_0) on the border of a scatterer B_0 with a velocity vector making a fixed angle θ_0 with the x-axis. The angle θ_0 would completely determine the direction of the trajectory *after* the reflection at ∂B_0, thus all our trajectories would arrive at a single point $X_0 \in \mathcal{M}$ determined by (x_0, y_0, θ_0); we will see under what conditions there might be more than one preimage of X_0 in $\mathcal{M}$.

Let the trajectory originate at a point (x, y) with initial velocity (u, v). Then by the rules (2.2) we have

$$x_0 = x + ut + \tfrac{1}{2}\varepsilon t^2, \qquad y_0 = y + vt$$

where t is the travel time. Note that $(u+\varepsilon t)/v = \cot\theta_0 =: k$, so that we can eliminate t and obtain

$$x = x_0 + \frac{u^2 - k^2 v^2}{2\varepsilon}, \qquad y = y_0 + \frac{uv - kv^2}{\varepsilon}. \tag{A.22}$$

Let us first suppose the particle starts with a unit speed, i.e., $u = \cos\theta$ and $v = \sin\theta$. Then x, y in (A.22) become functions of θ, and we get a one-parameter family of phase points that will arrive at the same collision point $X_0 \in \mathcal{M}$. By elementary calculation, all the points (x, y) lie on an ellipse E, and the corresponding outgoing velocity vectors (u, v) make a vector field on E transversal to E.

Now it is well possible that the boundary of another scatterer, B, crosses E more than once. Then from every point $(x, y) \in E \cap \partial B$ a trajectory may originate that is mapped by $\mathcal{F}_\varepsilon$ to X_0. Thus the collision map $\mathcal{F}_\varepsilon$ would take several points from the surface of the scatterer B to a single point $X_0 \in \mathcal{M}$. This means that the map $\mathcal{F}_\varepsilon$ would fail to be one-to-one even on the set of points that travel from one given scatterer, B, to another given scatterer, B_0. As a result, the map $\mathcal{F}_\varepsilon$ may create "wrinkles" and "folds" even within the domains where it is naturally continuous. The map $\mathcal{F}_\varepsilon$ may have infinite contraction rates within the domains of continuity, and its Jacobian may be zero at some points. All this would severely complicate our analysis of the hyperbolicity of $\mathcal{F}_\varepsilon$.

In order to avoid the above complications, let us abandon our assumption of the initial unit speed (i.e., $u = \cos\theta$ and $v = \sin\theta$) and return to the more general situation where (A.22) hold. There will be still a family of phase points (x, y, u, v) that arrive at the given point (x_0, y_0) with velocity directed at the given angle θ_0. Now a natural way to prevent the above complications (and guarantee that the map $\mathcal{F}_\varepsilon$ diffeomorphic on the set of points traveling from one given scatterer, B, to another given scatterer, B_0) is to make sure that this family of phase points is a single trajectory, i.e. $\dot{y}/\dot{x} = v/u$, where dots denote differentiation with respect to a family parameter. Differentiating (A.22) gives

$$\frac{\dot{u}v + u\dot{v} - 2kv\dot{v}}{u\dot{u} - k^2 v\dot{v}} = \frac{v}{u}$$

from which $\dot{v}(u - kv)^2 = 0$. Note that $u - kv = 0$ implies $x = x_0$ and $y = y_0$, which holds only at the last point (x_0, y_0). Thus in the rest of the family we must have $\dot{v} = 0$, hence, $v = \text{const}$ (the constant may depend on x_0, y_0, θ_0 and ε, of course). Combining with the first equation of (A.22) we obtain

$$\tfrac{1}{2}(u^2 + v^2) = \text{const} + \varepsilon x.$$

This means that the *total* energy must be kept constant. This brings us back exactly to the dynamics defined in Section 2.

References

[1] Alves J., Bonatti C., and Viana M., *SRB measures for partially hyperbolic systems whose central direction is mostly expanding*, Inv. Math. **140** (2000) 351–398.

[2] Baladi V. and Gouëzel S., *Good Banach spaces for piecewise hyperbolic maps via interpolation*, Annal. Inst. H. Poincaré **26** (2009), 1453–1481.

[3] Baladi V. and Gouëzel S., *Banach spaces for piecewise cone hyperbolic maps*, J. Modern Dynam. **4** (2010), 91–137.

[4] Bonetto F., Daems D. and Lebowitz J. L. *Properties of stationary nonequilibrium states in the thermostatted periodic Lorentz gas. I. The one particle system,* J. Statist. Phys. **101** (2000) 35–60.

[5] Brin M. and Stuck G., *Introduction to Dynamical Systems*, Cambridge U. Press, 2002.

[6] Bunimovich L. A. and Sinai Ya. G. *Statistical properties of Lorentz gas with periodic configuration of scatterers,* Comm. Math. Phys. **78** (1980/81), 479–497.

[7] Bunimovich L. A., Sinai Ya. G., and Chernov N. I. *Statistical properties of two-dimensional hyperbolic billiards,* Russ. Math. Surv. **46** (1991), 47–106.

[8] Chernov N. *Decay of correlations and dispersing billiards*, J. Stat. Phys. **94** (1999), 513–556.

[9] N. Chernov, *Sinai billiards under small external forces*, Ann. H. Poincaré **2** (2001), 197–236.

[10] Chernov N., *A stretched exponential bound on time correlations for billiard flows*, J. Statist. Phys., **127** (2007), 21–50.

[11] N. Chernov, *Sinai billiards under small external forces II*, Ann. H. Poincaré **9** (2008), 91–107.

[12] N. Chernov and D. Dolgopyat, *Brownian Brownian Motion – I*, Memoirs AMS, **198**, No 927 (2009), 193 pp.

[13] Chernov N., Dolgopyat D., *Galton Board: limit theorems and recurrence*, J. Amer. Math. Soc, **22** (2009), 821–858.

[14] N. Chernov and D. Dolgopyat, *Diffusive motion and recurrence on an idealized Galton Board*, Phys. Rev. Lett., **99** (2007), paper 030601.

[15] Chernov N., Dolgopyat D. *Anomalous current in periodic Lorentz gases with infinite horizon,* Russian Math. Surveys, **64** (2009), 73–124.

[16] Chernov N., Dolgopyat D. *Particle's drift in self-similar billiards*, Ergod. Th. Dynam. Syst., **28** (2008), 389–403.

[17] Chernov N., Markarian R. *Chaotic billiards,* Mathematical Surveys and Monographs **127** AMS Publishing Providence, RI, 2006. xii+316 pp.

[18] N. I. Chernov, G. L. Eyink, J. L. Lebowitz and Ya. G. Sinai, *Steady-state electrical conduction in the periodic Lorentz gas*, Comm. Math. Phys. **154** (1993), 569–601.

[19] N. I. Chernov, G. L. Eyink, J. L. Lebowitz and Ya. G. Sinai, *Derivation of Ohm's law in a deterministic mechanical model*, Phys. Rev. Lett. **70** (1993), 2209–2212.

[20] Chernov N. and Zhang H.-K., *Billiards with polynomial mixing rates.* Nonlineartity, **4** (2005), 1527–1553.

[21] C. P. Dettmann and G. P. Morriss, *Crisis in the periodic Lorentz gas*, Phys. Rev. E. **54** (1996), 4782–4790.

[22] Kornfeld I.P., Fomin S.V., and Sinai Ya.G., *Ergodic theory*, Springer Verlag, 1982.

[23] Gallavotti G. and Ornstein D., *Billiards and Bernoulli schemes*, Comm. Math. Phys. **38** (1974), 83–101.

[24] Galton F., *Natural Inheritance,* MacMillan, 1889 (facsimile available at www.galton.org).

[25] Lorentz H. A., *The motion of electrons in metallic bodies*, Proc. Amst. Acad. **7** (1905), 438–453.

[26] Melbourne I. and Török A. *Statistical limit theorems for suspension flows*, Israel J. Math. **144** (2004), 191–209.

[27] Moran B. and Hoover W., *Diffusion in a periodic Lorentz gas*, J. Stat. Phys. **48** (1987), 709–726.

[28] Ruelle D. *A review of linear response theory for general differentiable dynamical systems,* Nonlinearity **22** (2009) 855–870.

[29] Sinai Ya. G., *Dynamical systems with elastic reflections. Ergodic properties of dispersing billiards*, Russ. Math. Surv. **25** (1970), 137–189.

[30] Szász D. and Varjú T. *Limit Laws and Recurrence for the Planar Lorentz Process with Infinite Horizon,* J. Statist. Phys. **129** (2007), 59–80.

[31] L.-S. Young, *Statistical properties of dynamical systems with some hyperbolicity*, Ann. Math. **147** (1998) 585–650.

[32] L.-S. Young, *Recurrence times and rates of mixing*, Israel J. Math. **110** (1999), 153–188.

N. ChernovrDepartment of Mathematics, University of Alabama at Birmingham, Birmingham, AL 35294
e-mail: chernov@math.uab.edu

D. DolgopyatrDepartment of Mathematics, University of Maryland, College Park, MD 20742
e-mail: dmitry@math.umd.edu